The Company of **Biologists**

RESEARCH ARTICLE

Clathrin-mediated endocytosis is essential for the selective degradation of maternal membrane proteins and preimplantation development

Akihito Morita[1,2,*], Yuhkoh Satouh[1,*], Hidetaka Kosako[3], Hisae Kobayashi[1], Akira Iwase[2] and Ken Sato[1,‡]

ABSTRACT

Fertilization triggers significant cellular remodeling through the oocyte-to-embryo transition. In this transition, the ubiquitin-proteasome system and autophagy are essential for the degradation of maternal components; however, the significance of degradation of cell surface components remains unknown. In this study, we show that multiple maternal plasma membrane proteins, such as the glycine transporter GlyT1a, are selectively internalized from the plasma membrane to endosomes in mouse embryos by the late two-cell stage and then transported to lysosomes for degradation at the later stages. During this process, large amounts of ubiquitylated proteins accumulated on endosomes. Furthermore, the degradation of GlyT1a with mutations in potential ubiquitylation sites was delayed, suggesting that ubiquitylation may be involved in GlyT1a degradation. The clathrin inhibitor blocked GlyT1a internalization. Strikingly, the protein kinase C (PKC) activator triggered the heterochronic internalization of GlyT1a; the PKC inhibitor markedly blocked GlyT1a endocytosis. Lastly, clathrin inhibition completely blocked embryogenesis at the two-cell stage and inhibited cell division after the four-cell stage. These findings demonstrate that PKC-dependent clathrin-mediated endocytosis is essential for the selective degradation of maternal membrane proteins during oocyte-to-embryo transition and early embryogenesis.

KEY WORDS: Degradation, Embryogenesis, Endocytosis, Fertilization, PKC, Ubiquitylation

INTRODUCTION

After fertilization, zygotes drastically change their intracellular components for meiosis to those associated with mitotic cell division to initiate embryogenesis. This process is referred to as oocyte-to-embryo transition. Growing oocytes accumulate large amounts of proteins, mRNAs and other molecules as maternal components during the early developmental process. After fertilization, these maternal components are gradually degraded by the ubiquitin-proteasome system (UPS) and autophagy as zygotic/embryonic gene activation is initiated (Toralova et al., 2020). In the case of mouse embryogenesis, it has been reported that a population of maternal cytosolic proteins is polyubiquitylated in cells ranging from MII oocytes to early two-cell embryos and then degraded largely by the UPS at the four-cell stage (Shin et al., 2013). Autophagy is also induced immediately after fertilization and reactivated after the late two-cell stage to degrade maternal components (Tsukamoto et al., 2008). These degradation systems are essential for preimplantation development in mice (Shin et al., 2013; Toralova et al., 2020; Tsukamoto et al., 2008; Verlhac et al., 2010). However, the role, timing and mechanisms of endocytosis in the degradation of maternal plasma membrane proteins in mammalian embryogenesis remain unknown.

Protein degradation is tightly associated with the regulation of intracellular amino acid composition and plays an important role in supplying resources for *de novo* protein synthesis. In early mammalian embryogenesis, the transition from oocyte to embryo requires an energy source for drastic and morphological changes (Collado-Fernandez et al., 2012; Dumollard et al., 2009). Presumably, in response to the significant reconstruction of cellular components, oocytes and embryos have been reported to show the activation of various amino acid transport systems compared with their counterparts in somatic cells (Kandasamy et al., 2018) at distinct times during the oocyte-to-embryo transition (Pelland et al., 2009). Such amino acid transport systems are composed of specific transporters and regulatory proteins that localize to the plasma membrane to regulate amino acid transport between the cytoplasm and the extracellular environment (Kandasamy et al., 2018). For example, system Xc−, which consists of Slc7a11 (xCT) and Slc3a2, regulates the antiport of L-glutamate and L-cystine during the early stages of embryogenesis. System β consists of Slc6a6 (TAUT), which regulates the transport of taurine/β-alanine from the one-cell stage to the blastocyst stage, whereas system L, which consists of Slc7a5 (LAT1) and Slc3a2, functions as an antiporter for L-glutamine and L-leucine from the one-cell stage to the blastocyst stage of embryogenesis (Van Winkle et al., 1990, 1992, 1994). In addition to the importance of amino acid content regulation, certain amino acids, such as glycine and betaine, have been demonstrated to play essential roles in regulating the sizes of oocytes and embryos, acting as osmolytes, thereby maintaining the developmental ability of the embryo under various osmotic conditions (Anas et al., 2007; Baltz and Zhou, 2012). Several lines of evidence have shown that glycine concentration in the external environment is crucial for cell viability under hyperosmotic conditions during oogenesis and pre-implantation embryogenesis, especially during the early cleavage stages (Hadi et al., 2005; Steeves et al., 2003; Tartia et al., 2009). Glycine is transported by the glycine transporters GlyT1a and

[1]Laboratory of Molecular Traffic, Institute for Molecular and Cellular Regulation, Gunma University, Maebashi, 371-8512, Japan. [2]Department of Obstetrics and Gynecology, Gunma University Graduate School of Medicine, Maebashi, 371-8511, Japan. [3]Division of Cell Signaling, Fujii Memorial Institute of Medical Sciences, Institute of Advanced Medical Sciences, Tokushima University, Tokushima, 770-8503, Japan.
*These authors contributed equally to this work

‡Author for correspondence (sato-ken@gunma-u.ac.jp)

 A.M., 0000-0002-1443-2280; Y.S., 0000-0001-9207-9374; H.K., 0000-0003-3228-6368; K.S., 0000-0002-1034-5091

DEVELOPMENT

1

GlyT1b, which belong to the family of high-affinity Na^+- and Cl^--dependent neurotransmitter transporter proteins encoded by the *Slc6a9* gene (Guastella et al., 1992; Liu et al., 1993). GlyT1a is exclusively expressed in mammalian oocytes and early-stage embryos (Richard et al., 2017) and is involved in glycine transport during the oocyte-to-embryo transition (Van Winkle et al., 1988). These results indicate that GlyT1a is the only component that imports glycine to maintain both oocytes and embryos of an adequate size. Of these isoforms, GlyT1a mainly localizes to the plasma membrane in germinal vesicle (GV) and MI oocytes, as well as in early embryos before the compaction stage. Interestingly, GlyT1a is largely degraded after the compaction stage of pre-implantation embryonic development (Richard et al., 2017). However, how GlyT1a is removed from the cell surface of embryos has not yet been clarified.

Thus, in the present study, we established a non-invasive live imaging system for mouse embryogenesis and investigated the involvement of the endocytic pathway in the degradation of maternal membrane proteins during mammalian embryogenesis. Our study clearly demonstrated that protein kinase C (PKC)-triggered clathrin-mediated endocytosis is essential for the selective degradation of maternal plasma membrane proteins and appropriate preimplantation development.

RESULTS

Maternal membrane proteins are selectively endocytosed and degraded in lysosomes during embryogenesis

In rodents, the *Slc6a9* gene encodes GlyT1a and GlyT1b isoforms (Liu et al., 1993). Among these isoforms, GlyT1a is exclusively expressed in oocytes and early embryos, but is hardly detected at the blastocyst stage without elevated expression during early embryogenesis (Richard et al., 2017). To investigate the dynamics of GlyT1a during embryogenesis, we generated fluorescent protein-tagged mouse GlyT1a, which was fused with enhanced green fluorescent protein (EGFP) or mCherry at its C-terminus. The EGFP signal is quenched in lysosomes owing to the acidic environment but mCherry signal is not (Doherty et al., 2010). Thus, GlyT1a-EGFP and GlyT1a-mCherry are thought to emit green and red signals on their way to the lysosomes, respectively, but emit only red signals in acidic lysosomes. To follow the fate of GlyT1a after fertilization, we first synthesized GlyT1a-EGFP and GlyT1a-mCherry mRNAs and microinjected these mRNAs together into mouse one-cell-stage embryos (4 h post fertilization; hpf) and observed their expression and localization during early embryogenesis (Fig. 1A; Fig. S1). We found that both GlyT1a-EGFP and GlyT1a-mCherry were sufficiently expressed and largely localized to the plasma membrane by the late one-cell stage, and so
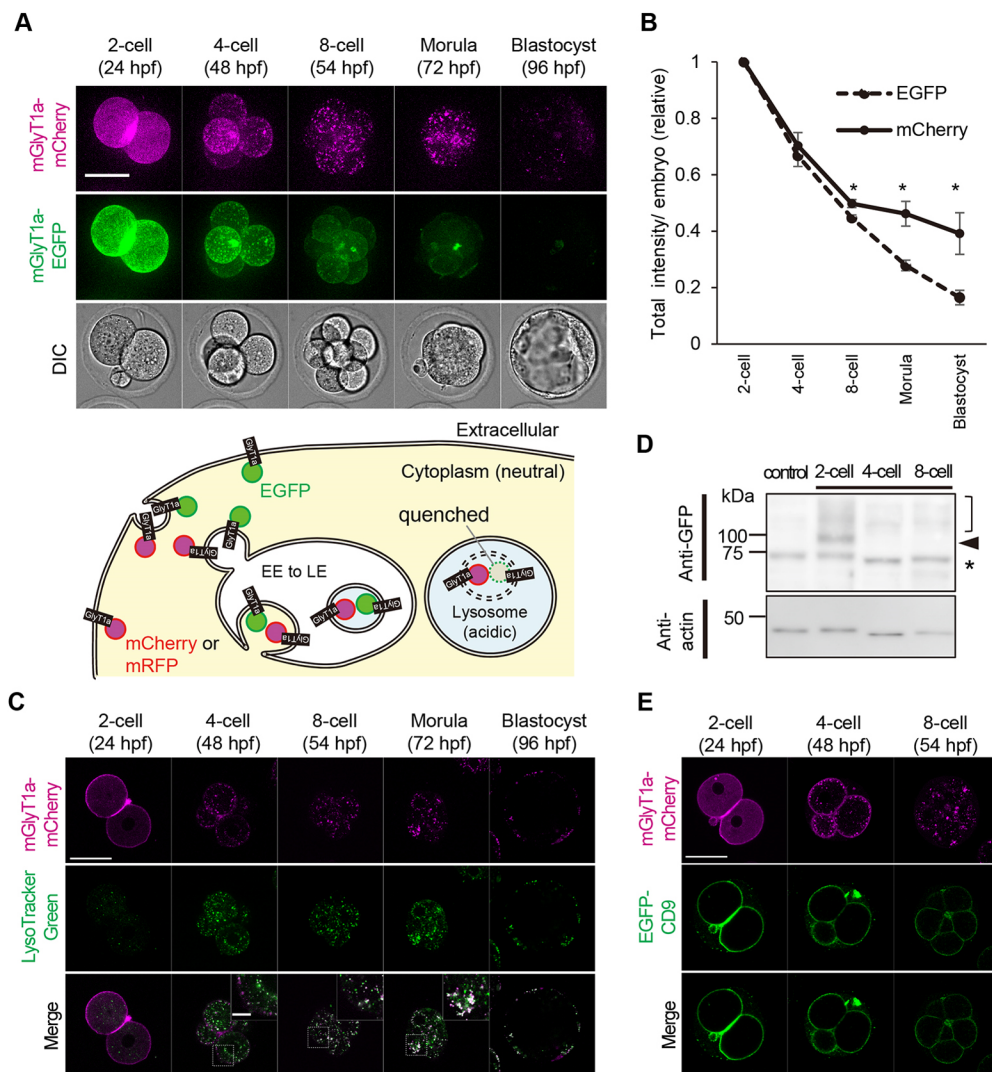

Fig. 1. GlyT1a is selectively endocytosed and degraded in lysosomes. (A) Top: Embryos expressing mGlyT1a-EGFP/mCherry were observed via laser confocal fluorescence microscopy (maximum intensity projection images indicated). DIC, differential interference contrast. Bottom: Schematic of pH-dependent quenching of EGFP fluorescence. (B) Relative fluorescent levels in the average intensity projection images of whole embryos at each stage. Data are representative of three independent experiments. (C) Embryos expressing mGlyT1a-mCherry were stained with LysoTracker Green and observed with laser confocal fluorescence microscopy (single *z*-plane slice indicated). (D) Embryos expressing mGlyT1a-EGFP/mCherry (40 embryos/lane) were immunoblotted using an anti-GFP antibody. Re-probed image obtained following treatment with an anti-actin antibody is also indicated. The control indicates non-injected two-cell embryos. The asterisk indicates a non-specific band. The arrowhead and square bracket indicate intact mGlyT1a-EGFP and its modified form, respectively. (E) CD9-EGFP Tg+*Cd9*$^{-/-}$ embryos expressing mGlyT1a-mCherry were observed using laser confocal fluorescence microscopy (single *z*-plane slice indicated). Regions in the white dotted frame are magnified in inset. *$P<0.05$ (two-tailed unpaired Student's *t*-test); error bars indicate s.e.m. Scale bars: 50 µm (insets: 10 µm).

we then examined the early phases of various developmental stages. At the four-cell stage, fluorescently tagged GlyT1a was transported to punctate structures in the cytoplasm, which are presumably endocytic compartments, and gradually disappeared by the blastocyst stage, as previously reported for endogenous GlyT1a (Richard et al., 2017), indicating that these fluorescently tagged GlyT1a mimicked intrinsic proteins. The number of GlyT1a-mCherry-positive punctate structures increased and peaked (∼300/embryo) at the four-cell stage, and the cytoplasmic signal remained even in blastocysts, whereas the GlyT1a-EGFP signal disappeared at the blastocyst stage (Fig. 1B; Fig. S2).

To examine whether GlyT1a is targeted to lysosomes during embryogenesis, we stained GlyT1a-mCherry-expressing embryos with LysoTracker Green, which labels acidic lysosomes (Fig. 1C). LysoTracker Green-positive lysosomes began to appear at the two-cell stage and emerged after the four-cell stage. GlyT1a-mCherry partly colocalized with lysosomes in four-cell-stage embryos and largely accumulated in lysosomes at the eight-cell stage, suggesting lysosomal targeting of GlyT1a during embryogenesis. We also examined the dynamics and amount of GlyT1a-EGFP by immunoblotting with an anti-GFP antibody. In lysates of GlyT1a-EGFP-expressing embryos obtained at each developmental stage, GlyT1a-EGFP was detected predominantly as a band with a molecular weight of approximately 97 kDa and as a high-molecular-weight species, which is presumably glycosylated or ubiquitylated (Barrera et al., 2015) (Fig. 1D, upper panel); its amounts decreased as embryogenesis proceeded. These results suggest that GlyT1a is endocytosed and degraded in lysosomes.

Next, we examined whether the internalization and degradation of GlyT1a during embryogenesis is a selective process. To test this, we compared the behavior of GlyT1a-mCherry with that of a GFP fusion protein with CD9, which is a tetraspanin family protein expressed on microvilli projected from the plasma membrane of oocytes and is required for efficient fertilization (Miyado et al., 2008). We found that EGFP-CD9, which was expressed maternally under the control of the *ZP3* promoter (Miyado et al., 2008), and GlyT1a-mCherry were mainly localized to the plasma membrane in early two-cell-stage embryos, whereas EGFP-CD9 remained on the plasma membrane even in four-cell and eight-cell embryos, in which GlyT1a-mCherry was already internalized (Fig. 1E).

We further investigated whether other maternal plasma membrane proteins are degraded during embryogenesis. To identify endogenous maternal plasma membrane proteins, we performed a proteomic analysis of mouse unfertilized oocytes. As a result, we identified various transmembrane proteins that were predicted to localize to the plasma membrane in mouse oocytes (Table S1). Among these proteins, we first observed the behavior of CD151, which belongs to the tetraspanin family, as well as of CD9 (Hasegawa et al., 1996), during embryogenesis. Interestingly, in contrast to CD9, fluorescently tagged CD151 was internalized from the plasma membrane at the early two-cell stage and degraded at later stages (Fig. S3A). Notably, the endocytosis of fluorescently tagged CD151 began slightly earlier than that of fluorescently tagged GlyT1a (Fig. S3A). We also examined the behavior of synaptophysin-like protein (Sypl), a multi-spanning membrane protein (Haass et al., 1996), during embryogenesis. We found that the fluorescently tagged Sypl was endocytosed and targeted to lysosomes at a similar time to fluorescently tagged GlyT1a (Fig. S3B). These results suggest that multiple maternal plasma membrane proteins are selectively endocytosed at different times during the two-cell stage and delivered to lysosomes for degradation.

RAB5 and RAB7 colocalize immediately after fertilization and start to segregate after the two-cell stage

The endocytosis of plasma membrane proteins is regulated by several RAB small GTPases, such as RAB5 and RAB7 (Langemeyer et al., 2018). RAB5 and RAB7 are mainly localized to early endosomes and late endosomes at a steady state, respectively, and the sequential conversion of RAB5 to RAB7 on endosomes plays a key role in endocytic lysosomal degradation (Rink et al., 2005). However, to date, no study has examined the dynamics of RAB5 and RAB7 in mammalian embryos. Thus, we explored whether the exogenous expression of EGFP- or mRFP-tagged RAB5A or RAB7A affects embryonic development and viability. To this end, we microinjected mRNAs of EGFP- or mRFP-tagged human RAB5A and RAB7A into embryos at 4 hpf. The embryos expressing these proteins were found to be largely viable and showed a superficially normal embryonic developmental ability to the blastocyst stage compared with control embryos (Fig. S4). The fluorescence levels of EGFP-hRAB5A and EGFP-hRAB7A in embryos decreased gradually as
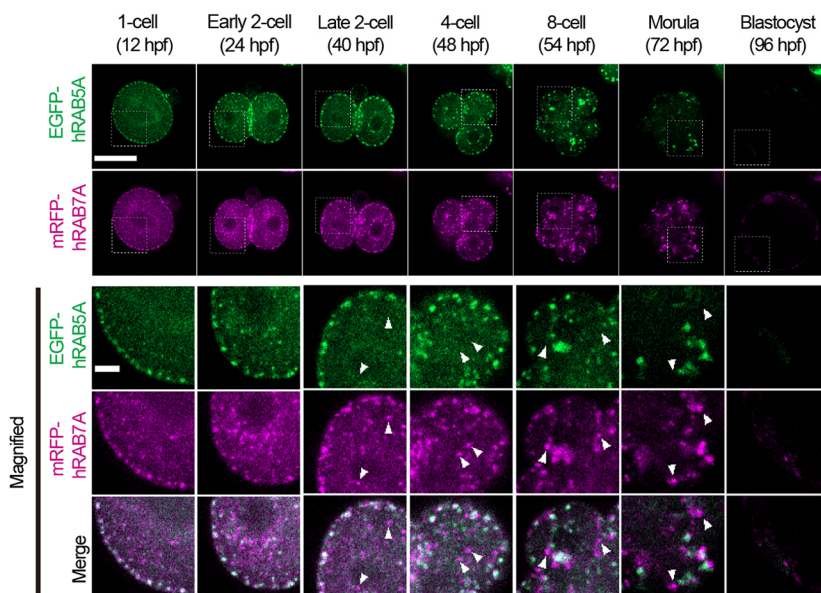

Fig. 2. Endosomal maturation is developmentally regulated during embryogenesis. Embryos expressing EGFP-hRAB5A and mRFP-hRAB7A were continuously observed via a low-invasive imaging system. Single z-plane slices of same embryo are indicated. Regions in the white dotted frame in the top panels are magnified in the bottom panels. The arrowheads indicate RAB5-negative and RAB7-positive endosomes showing segregation of RAB5 and RAB7. Scale bars: 50 μm (magnified: 10 μm).

DEVELOPMENT

3

embryogenesis proceeded, presumably owing to the dilution and/or turnover of exogenously introduced mRNA and its translation products (Fig. S5). Notably, when the same amount of mRNA was introduced into the embryos, the degradation rate of EGFP-hRAB5A and hRAB7A were significantly lower than that of Glty1a-EGFP in the four-cell, eight-cell, and morula stages, suggesting that GlyT1a is more actively degraded than cytosolic RAB proteins during embryogenesis. When both EGFP-hRAB5A and mRFP-hRAB7A mRNAs were microinjected into embryos, these proteins appeared on cortical punctate structures at the one-cell stage and colocalized with each other frequently up to the early two-cell stage, whereas they started to segregate with hRAB7A-specific punctate structures that emerged in the cytoplasm during the two-cell stage (Fig. 2; Fig. S6). We confirmed that endogenous RAB5 and RAB7 exhibit similar behavior in untreated early embryos at each developmental stage by immunostaining with specific antibodies (Fig. S7). Lastly, EGFP-hRAB5A and mRFP-hRAB7A were found to localize to larger puncta distributed throughout the cytosol in the later stages, suggesting that endosomal biogenesis is developmentally regulated.

GlyT1a is endocytosed via RAB5- and RAB7-positive endosomes

Next, we studied the transport kinetics of GlyT1a through endocytic compartments during embryogenesis using a low-invasive imaging system (Fig. 3). GlyT1a-mCherry began to localize to EGFP-hRAB5A-positive early endosomes in late two-cell-stage embryos (40 hpf), and this colocalization peaked at the four-cell stage (48 hpf) (Fig. 3A,C; Movie 1). GlyT1a-mCherry was then transported to EGFP-hRAB7A-positive late endosomes from the four-cell stage (48 hpf) to the eight-cell stage (54 hpf) and was still detected on these structures even in morula-stage embryos (72 hpf) (Fig. 3B,D; Movie 2), suggesting that the endocytic trafficking of GlyT1a is regulated by RAB5A and RAB7A. During early embryogenesis, GlyT1a-positive puncta (~100/embryo) overlapped with RAB5A-positive-early endosomes (~300/embryo) at the four-cell stage, whereas GlyT1a-positive puncta (~120/embryo) colocalized with RAB7A-positive late endosomes (~240/embryo) at the eight-cell stage (Fig. S8; Movie 3). Consistent with the immunoblotting results (Fig. 1D), a shift in the membranous to luminal localization of GlyT1a-mCherry was observed after the eight-cell stage (Fig. S9), indicating degradation of the native GlyT1a-mCherry form (Fig. 1A). Notably, the transport kinetics of GlyT1a through the endocytic pathway was quite slow during embryogenesis compared with that in neural cells or somatic cells (Fernández-Sánchez et al., 2009; Vargas-Medrano et al., 2011).

Massive accumulation of ubiquitylated proteins on endosomes occurs transiently in oocytes and embryos

As the selective degradation of plasma membrane proteins is regulated by ubiquitylation, we hypothesized that intracellular
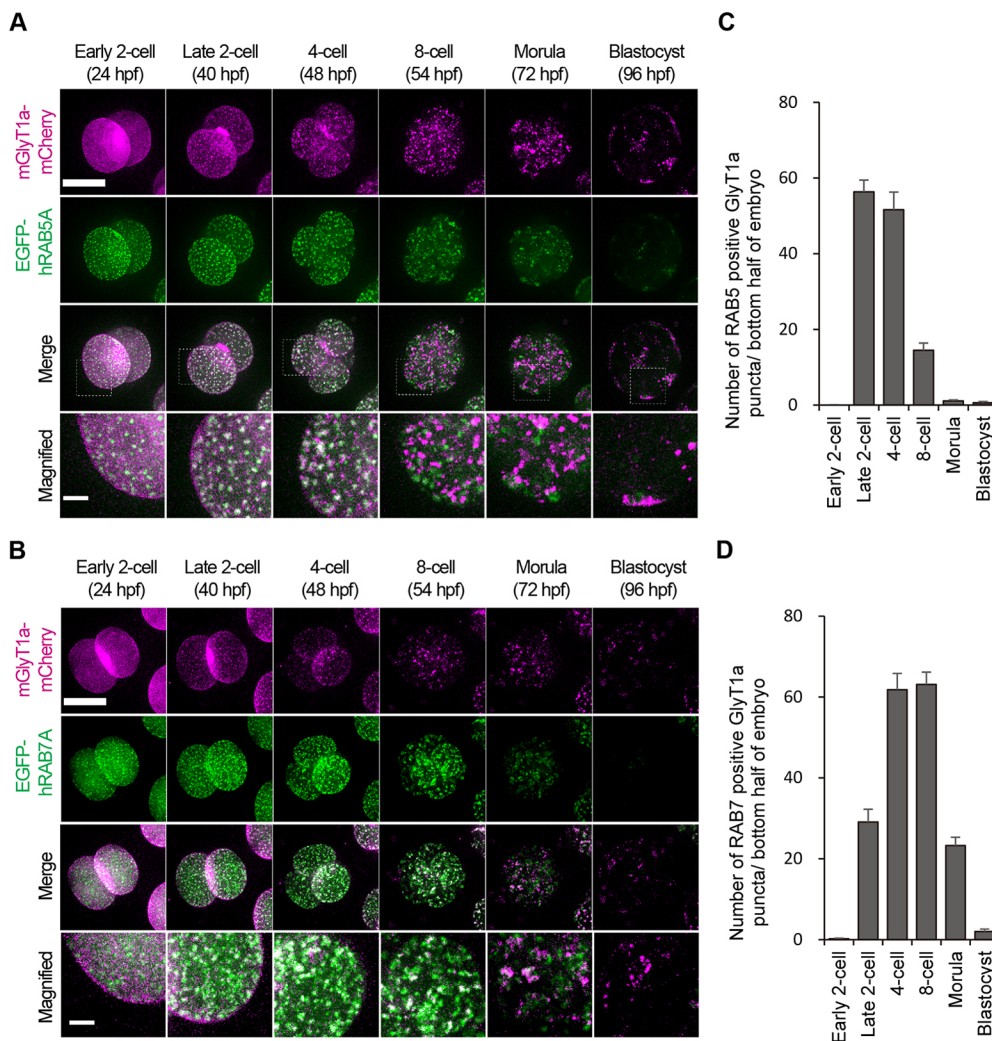

Fig. 3. GlyT1a starts to be endocytosed at the late two-cell stage and delivered to late endosomes by the eight-cell stage. (A,B) Embryos expressing EGFP-hRAB5A or EGFP-hRAB7A and mGlyT1a-mCherry were continuously observed via a low-invasive imaging system. Regions in the white dotted frame are magnified in the bottom panels. (C,D) Numbers of RAB5- or RAB7-positive puncta colocalized with GlyT1a in A or B were counted using the JACoP plugin of ImageJ. The error bars indicate s.e.m. Scale bars: 50 μm (magnified: 10 μm).

ubiquitylation is upregulated upon the endocytosis of maternal plasma membrane proteins. Certain maternal membrane proteins in *Caenorhabditis elegans* are internalized and selectively degraded in lysosomes in one-cell-stage embryos (Sato et al., 2006, 2008). In this process, a drastic accumulation of ubiquitylated proteins on endosomes occurs in one-cell-stage embryos (Sato et al., 2014). To examine whether the accumulation of ubiquitin signals on endosomes also occurs in mouse embryos, we immunostained mRFP-hRAB5A-expressing embryos with an anti-ubiquitin antibody (FK2) that recognizes ubiquitin conjugated to proteins but not free ubiquitin (Fujimuro and Yokosawa, 2005; Sato et al., 2014). The FK2 antibody has been widely used for the immunostaining and immunoblotting of poly-ubiquitin chains to analyze the dynamics of ubiquitylated proteins during endocytic pathway (Sato et al., 2014; van Wijk et al., 2019). We detected the ubiquitin signal on mRFP-hRAB5A-positive cortical early endosomes and enlarged early endosomes in one-cell- and two-cell-stage embryos, respectively (Fig. 4A). The ubiquitin staining signal colocalized with GlyT1a-mCherry-positive punctate structures underneath the plasma membrane in two-cell-stage embryos and overlapped with endocytosed GlyT1a-mCherry in four-cell-stage embryos, suggesting that GlyT1a-mCherry is subjected to ubiquitylation after fertilization (Fig. 4B). We also found that mRFP-CD151 and mRFP-Sypl overlapped with FK2-labeled ubiquitin-positive punctate structures directly beneath the plasma membrane in two-cell-stage embryos (Fig. S10), suggesting that ubiquitylation is commonly involved in the degradation of maternal plasma membrane proteins.

As the ubiquitylation of cytoplasmic lysine residues on GlyT1 has been reported to function as a sorting signal for lysosomal degradation in somatic cells (Barrera et al., 2015; Fernández-Sánchez et al., 2009), we generated a GlyT1a-7KR-EGFP mutant, in which all lysine residues in the N- and C-terminal cytosolic regions were replaced with alanine residues, and its degradation rate

was monitored during embryogenesis. Although the total EGFP fluorescence intensities of both GlyT1a-EGFP (WT; wild-type) and GlyT1a-7KR-EGFP were gradually reduced and almost disappeared at the blastocyst stage, most likely owing to mRNA turnover and protein dilution, the degradation rate of GlyT1a-7KR-EGFP was significantly low ($P=0.018$ and $P<0.001$ at the four-cell and eight-cell stages, respectively) compared with that of GlyT1a-EGFP (Fig. 4C,D), suggesting that the lysine residues on GlyT1a are important for lysosomal degradation.

PKC triggers clathrin-mediated endocytosis during embryogenesis

To determine whether the internalization of GlyT1a is clathrin-dependent, we examined the internalization of a fluorescently tagged GlyT1a in the presence of the clathrin inhibitor, Pitstop2 (von Kleist et al., 2011). As expected, this treatment completely blocked the internalization of GlyT1a from the plasma membrane at the late two-cell stage (Fig. 5A,B). We also examined the effect of Dynasore, an inhibitor of dynamin, which regulates broad types of dynamin-related endocytosis (Mayor et al., 2014) on Glyt1a trafficking. We found that Dynasore inhibited the endocytosis of GlyT1a-EGFP (Fig. S11) and also blocked the cell division of two-cell-stage embryos as reported previously (Wang et al., 2015). These results suggest that GlyT1a is endocytosed via a clathrin-dependent mechanism.

It has been reported that the endocytosis of GlyT1a in somatic cells is regulated by PKC (Vargas-Medrano et al., 2011). To test the involvement of PKC in the internalization of GlyT1a during embryogenesis, we first treated one-cell stage-embryos with a PKC activator, Phorbol 12-Myristate 13-Acetate (PMA). Interestingly, PMA treatment resulted in a heterochronic targeting of GlyT1a-EGFP and GlyT1a-mCherry to endosomes, even at the one-cell stage, when these proteins largely remained on the plasma membrane in the control embryos (Fig. 5C,D). Next, we treated
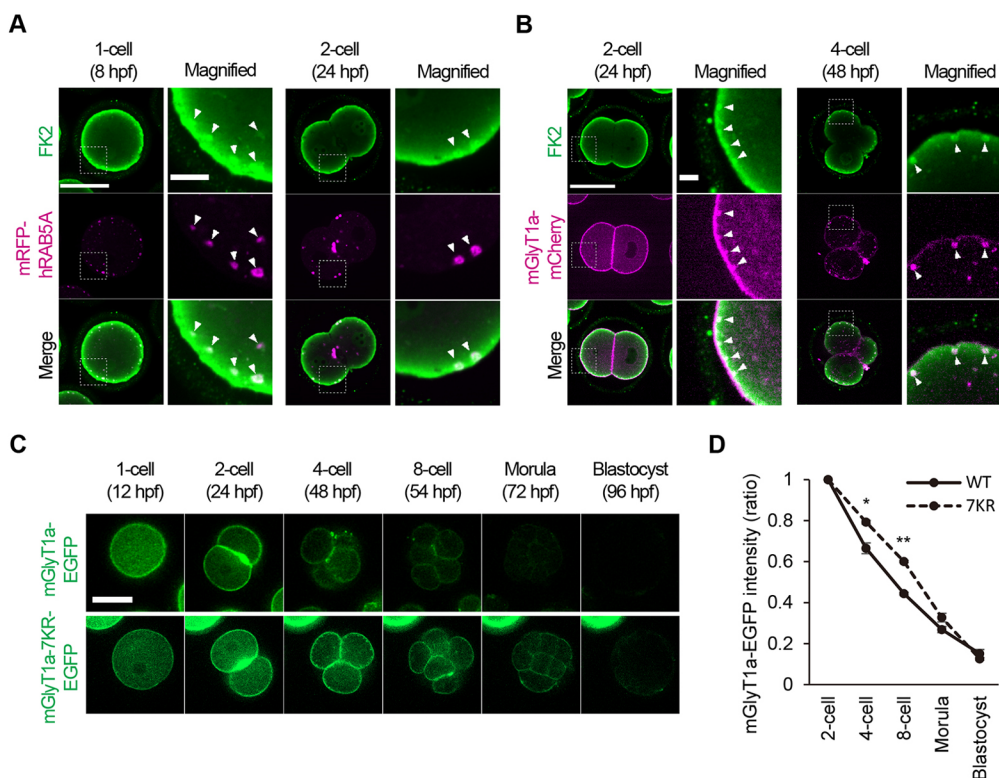

Fig. 4. A massive accumulation of ubiquitylated proteins on endosomes takes place in early embryos. (A) Embryos expressing mRFP-hRAB5A were fixed and stained with an anti-ubiquitin antibody (FK2; green). (B) Embryos expressing mGlyT1a-mCherry were fixed and stained with an anti-ubiquitin antibody (FK2; green). The arrowheads indicate punctate structures showing accumulation and colocalization. Regions in the white dotted frame are magnified in the right-hand panels. (C) Embryos expressing mGlyT1a-7KR-EGFP or mGlyT1a-EGFP were continuously observed via a low-invasive imaging system. (D) Relative fluorescent levels of average intensity projection images of whole embryos at each stage. Data are representative of three independent experiments. *$P<0.05$, **$P<0.01$ (two-tailed unpaired Student's t-test); the error bars indicate s.e.m. Single confocal z-plane slices are indicated. Scale bars: 50 µm (magnified: 10 µm).
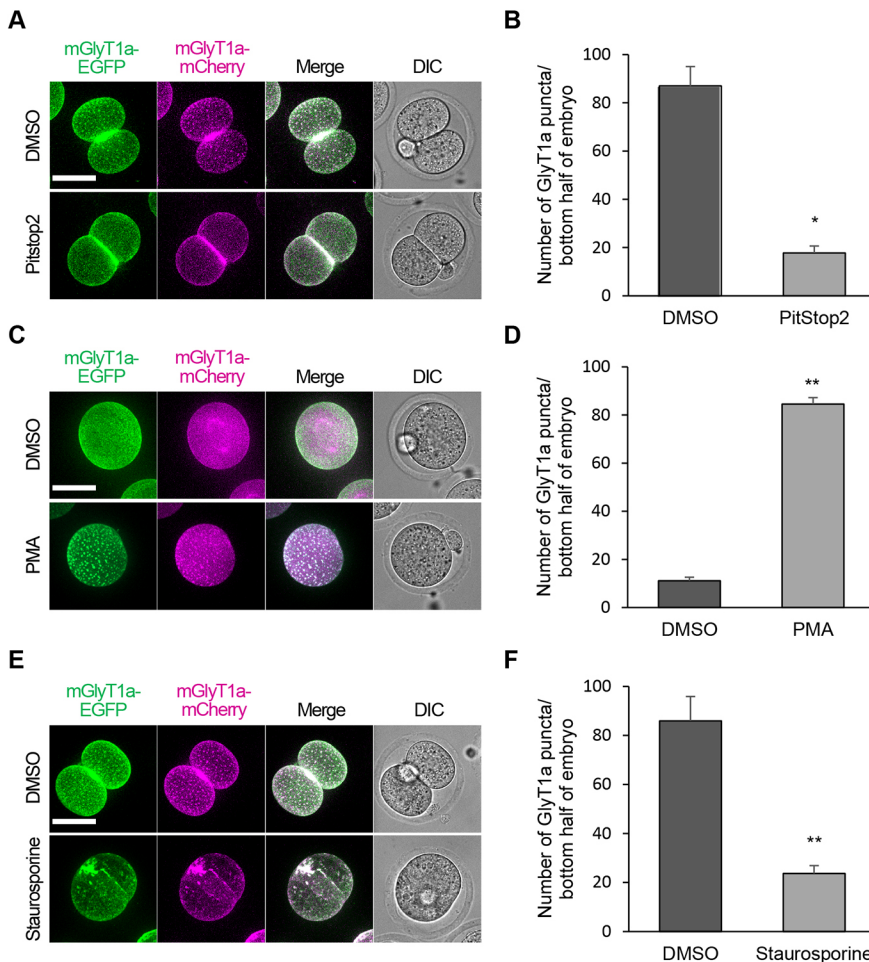
Fig. 5. PKC triggers clathrin-mediated endocytosis of GlyT1a. (A) Embryos expressing mGlyT1a-EGFP/mCherry at 22 hpf were cultured for 18 h in the presence or absence of Pitstop2. (B) The number of mGlyT1a puncta after the culture in A were counted. (C) Embryos expressing mGlyT1a-EGFP/mCherry at 8 hpf were cultured for 10 h in the absence or presence of PMA. (D) The number of mGlyT1a puncta after the culture in C were counted. (E) Embryos expressing mGlyT1a-EGFP/mCherry at 22 hpf were cultured for 18 h in the presence or absence of Staurosporine. (F) The number of mGlyT1a puncta after the culture in E were counted. $*P<0.05$, $**P<0.01$ (two-tailed unpaired Student's t-test); the error bars indicate s.e.m. A, C and E show maximum intensity projections of confocal micrographs. Scale bars: 50 μm.

the embryos with the PKC inhibitor Staurosporine at the early two-cell stage and examined whether GlyT1a was targeted to the endosomes at the late two-cell stage. This treatment significantly inhibited the targeting of fluorescently labeled GlyT1a to punctate structures and caused the accumulation of these proteins in aberrant structures around the cell division plane (Fig. 5E,F).

Clathrin-mediated endocytosis is essential for early embryonic development

Finally, we studied whether clathrin-mediated endocytosis is required for early development. To test this, we treated embryos at various stages with Pitstop2 and observed its effects on early embryogenesis (Fig. 6A-C). When embryos were treated with Pitstop2 from the one-cell stage (8 hpf), these embryos largely developed to the two-cell stage at 24 hpf. However, when we treated early two-cell-stage embryos with Pitstop2, these embryos failed to develop into the four-cell stage. In addition, Pitstop2 treatment at the four-cell stage significantly decreased the number of embryos developing into the eight-cell, morula and blastocyst stages. Notably, the number of cells composing the morula and blastocyst, which were developed from embryos treated with Pitstop2 at the four-cell stage, was significantly lower than that in control embryos, although most of such embryos underwent compaction (Fig. 6D,E). By contrast, Pitstop2 treatment from the eight-cell stage gave subtle effects on later developmental stages (Fig. 6B,C). The stage-specific effects of Pitstop2 treatment suggest that clathrin-mediated endocytosis is crucial, especially in the two-cell to the four-cell stages of early embryogenesis.

DISCUSSION

GlyT1a plays an important role on the surface of the embryo in regulating osmotic pressure during early embryogenesis (Hadi et al., 2005; Tartia et al., 2009). In this study, based on the analysis of the dynamics of this molecule, we showed that GlyT1a is selectively internalized and actively degraded in lysosomes by clathrin-mediated endocytosis during early embryogenesis. Assays using PKC activator/inhibitor demonstrated that GlyT1a endocytosis is regulated by PKC activity, as reported for somatic cells (Vargas-Medrano et al., 2011). We also found that a high level of accumulation of ubiquitylated proteins in endosomes transiently occurs in early-stage embryos. Finally, we showed that clathrin-mediated endocytosis is essential for early embryogenesis, especially in the progression from the two-cell stage to the four-cell stage, when the oocyte-to-embryo transition actively proceeds (Fig. 6F).

GlyT1a is the main transporter that delivers glycine to mammalian oocytes and embryos (Van Winkle et al., 1988). The removal of GlyT1a from the plasma membrane at the late two-cell stage should fundamentally change the characteristics of the response to the surrounding environment and the amino acid requirements of embryos. Interestingly, the second activation of autophagy also occurs at the late two-cell stage, suggesting that the degradation of maternal cytoplasmic proteins is highly upregulated at this point as well. Selective elimination of amino acid transporters such as GlyT1a from the plasma membrane may result in the transient depletion of certain amino acids that are coupled to the induction of autophagy during embryogenesis.
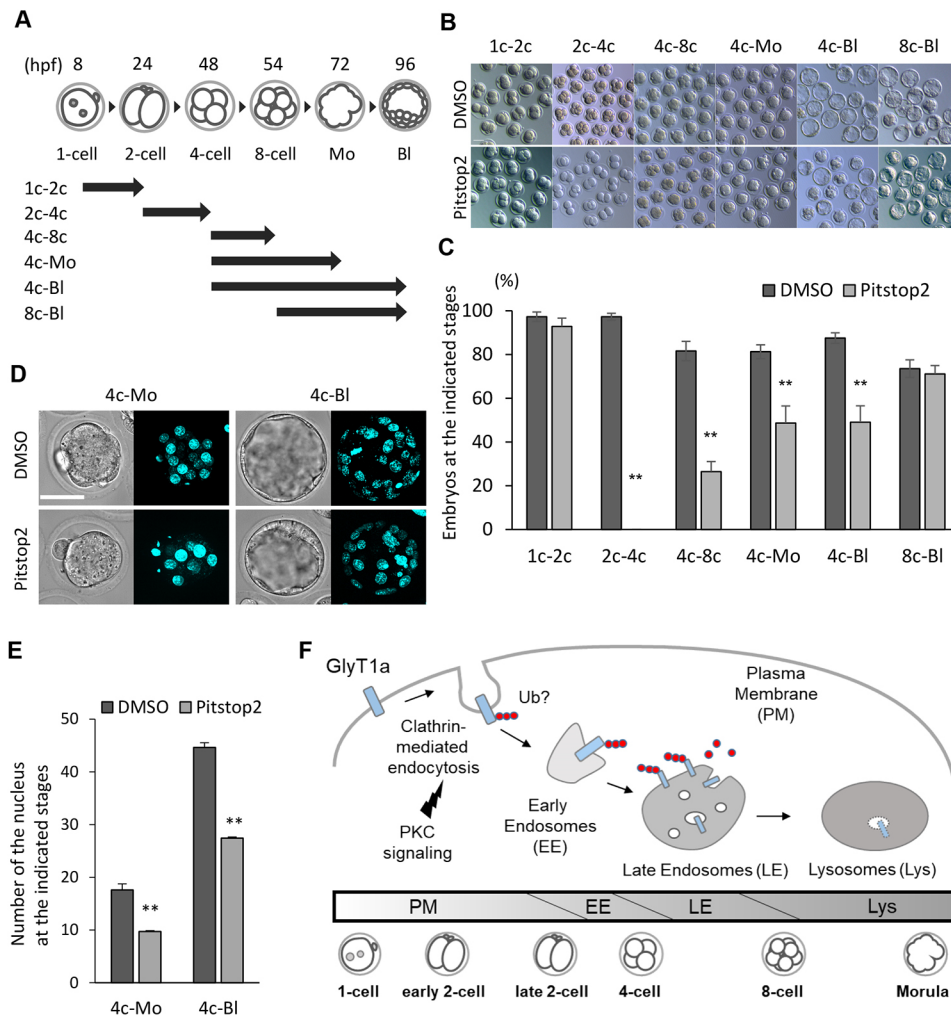
Fig. 6. Clathrin-mediated endocytosis is essential for embryonic development. (A) Schematic indicating the time course of Pitstop2 treatments performed in this study. (B,C) Representative images (B) and quantification (C) showing rate of development of embryos developed to the indicated stages after Pitstop2 treatment. Data are representative of three independent experiments. (D,E) Representative images (D) and quantification (E) showing the number of nuclei at the morula (4c-Mo) or blastocyst (4c-Bl) stage after Pitstop2 treatment. Nuclei were stained with Hoechst 33342. (F) Schematic summarizing this study. **$P<0.01$ (two-tailed unpaired Student's t-test); the error bars indicate s.e.m. Scale bars: 50 μm.

We identified a large accumulation of ubiquitylated proteins on endosomes in early mammalian embryos, suggesting that multiple maternal plasma membrane proteins (apart from GlyT1a) are ubiquitylated for efficient degradation in lysosomes. In fact, an EGFP-tagged GlyT1a-7KR-mutant, in which all lysine residues in the cytoplasmic regions were mutated, was degraded significantly slower than WT GlyT1a-EGFP, although its signal finally disappeared in blastocysts. We also found that fluorescently labeled CD151 and Sypl were endocytosed for lysosomal degradation during the two-cell stage of embryogenesis. Among these proteins, the degradation of CD151 is accelerated by the ubiquitylation of cytoplasmic tails in cultured cells (Lineberry et al., 2008). Notably, CD151 was endocytosed from the plasma membrane slightly earlier than GlyT1a, suggesting that the ubiquitylation of these proteins is regulated by different mechanisms. In contrast, CD9, which is mainly localized to the plasma membrane and contributes to the maintenance of microvilli structures on the cell surface of oocytes and embryos (Miyado et al., 2008; Umeda et al., 2020), remained on the plasma membrane even at the eight-cell stage, indicating that this process is selective. Further experiments are needed to clarify the difference between CD9 and other maternal plasma membrane proteins that are endocytosed for lysosomal degradation.

Activation and inhibition of PKC promoted and suppressed the internalization of GlyT1a during embryogenesis. These results suggest that PKC-dependent mechanisms regulate the clathrin-mediated endocytosis of GlyT1a after fertilization. Interestingly,

we previously reported that certain maternal membrane proteins are selectively ubiquitylated and degraded via endocytosis immediately after fertilization in *C. elegans* embryos, suggesting that this process is well conserved from worms to mammals (Sato et al., 2006, 2014).

The development of a low-invasive live imaging system allowed us to observe the biogenesis of endosomes and lysosomes and protein transport through the endocytic pathway during embryogenesis. In one-cell-stage embryos, fluorescently tagged hRAB5A and hRAB7A were mainly localized to cortical punctate structures, which were segregated and redistributed to the cytoplasm during the two-cell stage and became enlarged after the four-cell stage. Interestingly, such punctate structures were hardly stained with LysoTracker Green, which labels acidic lysosomes, by the two-cell stage, suggesting that lysosomal maturation starts to occur after the two-cell stage, as reported previously (Tsukamoto et al., 2013). These findings indicate that the biogenesis and maturation of endosomes/lysosomes are highly regulated during early embryogenesis. We also noticed that the transport kinetics of GlyT1a from hRAB5A-positive early endosomes to hRAB7A-positive late endosomes during embryogenesis was quite slow compared with that in somatic cells (Fig. 3; Rink et al., 2005). It is possible that RAB conversion is a developmentally regulated limiting step for the progression from early to late endosomes during embryogenesis.

In summary, our findings show the importance of clathrin-mediated endocytosis especially at the two-cell and four-cell stages

of mouse embryogenesis. We also gained new insights into the efficient degradation system for maternal membrane proteins that can determine the mode of embryonic amino acid metabolism and developmental ability. For assisted reproductive technologies, including *in vitro* fertilization, it is important to select embryos that have the best chance of developing into healthy offspring to improve the probability of pregnancy. Given the crucial role of clathrin-mediated endocytosis in embryonic development, the assessment of endocytic activity in individual embryos could be used to select embryos that show enhanced embryonic development and high pregnancy rates. To achieve this, further analyses of the dynamics of other plasma membrane proteins and the precise molecular mechanisms underlying endocytosis are required.

MATERIALS AND METHODS

Mice and embryo culture
All experimental protocols involving animals were approved and performed in accordance with the guidelines of the Animal Care and Experimentation Committee of Gunma University (Approval No. 19-001). Hybrid B6D2F1 male and female mice were purchased from the Japan SLC. The C57BL/6-CD9TMLTg (ZP3-EGFP CD9) transgenic mice were gifted by Dr Kenji Miyado of the National Research Institute for Child Health and Development, Tokyo. All animals were >8 weeks old.

Construction of plasmids
The constructs for expression in mammalian cells and *Escherichia coli* were prepared using the Gateway recombination cloning technology (11789-013 and 11791-019; Invitrogen). *mGlyT1a* cDNA (UniProt accession number P28571) from the mouse embryo cDNA library (DLM110; OriGene Technologies) was amplified using PCR. The amplified DNA fragment was then subcloned into the pDONR221 entry vector and transferred into the destination vector pDEST-CMV-C-EGFP or pDest-mCherry-N1 (Addgene #122844 and #31907, respectively) using Gateway recombination cloning technology for the expression of the C-terminal EGFP or mCherry-tagged proteins, respectively. Open reading frames of human RAB5A and RAB7A proteins (UniProt accession numbers P20339 and P51149, respectively) were amplified using PCR, as previously described (Sakaguchi et al., 2015). The amplified DNA fragments were then subcloned into the pDONR221 entry vector (12536017; Invitrogen) and transferred into the destination vector pcDNA3.1 (V790-20; Invitrogen) for the expression of the N-terminal EGFP or mRFP-tagged proteins, as described above. *mCD151* cDNA (UniProt accession number O35566) and *mSypl* cDNA (UniProt accession number O09117) from the mouse ovary cDNA library (MD-15; GenoStaff) were amplified using PCR. The amplified DNA fragments were subcloned into the pDONR221 entry vector and transferred into the destination vector pcDNA3.1 to express the N-terminal EGFP or mRFP-tagged proteins. Multiple lysine substitutions of GlyT1a were designed according to the method described by Barrera (Barrera et al., 2015). Mutations were introduced using the Q5 Site-Directed Mutagenesis Kit following the manufacturer's protocol (E0552S; New England Biolabs). All experimental protocols were approved by the Gunma University Genetic Modification Safety Committee (approval no. 19-027).

RNA synthesis and microinjection
T7 promoter-tagged cDNAs were amplified using PCR with High-fidelity Taq polymerase, KOD FX Neo (KFX-201; Toyobo). For the N-terminal EGFP-tagged proteins (EGFP-hRAB5A, EGFP-hRAB7A, EGFP-Sypl, and EGFP-CD151) and N-terminal mRFP-tagged proteins (mRFP-hRAB5A, mRFP-hRAB7A, mRFP-Sypl, mRFP-CD151) in the pcDNA3.1 backbone, the primers 5′-GCGCTAATACGACTCACTATAGGGAGACCCAA-3′ and 5′-GACTCGAGCGGCCGCCACTGTGCTGGAT-3′ were used. For mGlyT1a-EGFP, primers 5′-GGTAATACGACTCACTATAGGGGC-CGCCATGGTAGGAAAAGGTGCCAAAG-3′ and 5′-TAGAAGGCAC-AGTCGAGG-3′ were used. For mGlyT1a-7KR-EGFP, primers 5′-GG-TAATACGACTCACTATAGGGGCCGCCATGGTAGGAAGAGGT-GCCAGA-3′ and 5′-TAGAAGGCACAGTCGAGG-3′ were used.

For mGlyT1a-mCherry, primers 5′-GGTAATACGACTCACTA-TAGGGGCCGCCATGGTAGGAAAAGGTGCCAAAG-3′ and 5′-GAAATTTGTGATGCTATTGC-3′ were used. RNA synthesis using each PCR amplicon as template, poly A tail addition, and further preparation for egg injection were performed as previously described (Umeda et al., 2020), using an mMESSAGE mMACHINE T7 kit (AM1344; Invitrogen) and a Poly(A) Tailing kit (AM1350; Invitrogen), according to the manufacturer's protocols. All the injection experiments were carried out using 100 ng/µl of mRNA in RNase-free demineralized water. Microinjection was performed using a piezo-micromanipulator with a glass capillary needle under an inverted microscope, as previously described (Satouh et al., 2017).

Antibodies and chemicals
The following antibodies were used: mouse monoclonal anti-GFP antibody (Clones 7.1, 13.1; 11814460001; Roche), mouse monoclonal anti-actin antibody (C4; MAB1501; Millipore), mouse monoclonal anti-multi-ubiquitin antibody (FK2; D058-3; Medical & Biological Laboratories), rabbit monoclonal anti-RAB5 antibody (C8B1; Cell Signaling Technology) and rabbit monoclonal anti-RAB7 antibody (D95F2; Cell Signaling Technology).

Pitstop2, a cell-permeable clathrin inhibitor, was purchased from Abcam (ab120687). Phorbol 12-myristate 13-acetate (PMA), potent PKC activator, was purchased from Selleck Biotech (S7791). Staurosporine, a potent PKC inhibitor, was purchased from MedChemExpress (HY-15141). Dimethyl sulfoxide (DMSO) was purchased from Nacalai Tesque (13406-55). Dynasore, a dynamin inhibitor, was purchased from Sigma-Aldrich (D7693).

Immunoblotting
Forty embryos microinjected with *mGlyT1a-EGFP* mRNA were collected at the indicated stages and washed four times in phosphate-buffered saline (PBS) containing polyvinyl alcohol (PVA/PBS). The cells were then lysed in 2× Laemmli sample buffer. These samples were separated using sodium dodecyl sulfate polyacrylamide gel electrophoresis (10% gel) and transferred onto polyvinylidene fluoride membranes. The membranes were probed with an anti-GFP antibody or anti-actin antibody described above (1:1000 for both), followed by treatment with horseradish peroxidase-conjugated secondary antibody (1:5000; 115-035-003; Jackson ImmunoResearch).

Confocal microscopy and immunostaining
Fluorescent images were obtained using a confocal microscope system FV1200 (Olympus) for single slices and CSU-W1 (Yokogawa Electric Corporation) for whole oocytes/embryos. Oocytes or embryos (microinjected with mRNA) were cultured to the indicated stages and fixed in 4% paraformaldehyde in PVA/PBS for 15 min at 25-27°C. After fixation, the cells were permeabilized with 0.1% Triton X-100 in PVA/PBS for 30 min at room temperature, and washed three times with PVA/PBS. After blocking with 5% fetal bovine serum (FBS) in PBS for 30 min at room temperature, the cells were incubated with the primary antibodies described above (1:100 for all) overnight at 4°C. Next, they were washed three times in PVA/PBS, and incubated with anti-mouse or rabbit IgG secondary antibodies coupled with Alexa Fluor 488 (1:200 for both; A32723 for anti-mouse and A32731 for anti-rabbit; Thermo Fisher Scientific) at 25-27°C for 6 h. Then, the cells were washed with fresh PVA/PBS three times. Control, non-specific staining, was performed by processing the oocytes and embryos as described above, but in the absence of a primary antibody. The oocytes and embryos were photographed in microdrops of PVA/PBS on glass-bottomed dishes under a confocal microscope.

Low-invasive fluorescent imaging
Low-invasive fluorescent imaging of embryos was performed as previously described (Satouh et al., 2017; Yamagata et al., 2009). Microinjection of mRNAs was carried out at 4 hpf, and the embryos were cultured in CARD KSOM medium (Kyudo). Confocal images at 41 z-axis planes with 2 µm increments for both a 488-nm (EGFP) and 561-nm (mCherry, mRFP) laser were obtained every 20 min using a Yokogawa confocal scanner unit CV1000. Analysis of the acquired images, including background

subtraction and intensity quantification of the averaged *z*-stack projection images, was performed using ImageJ software.

In vitro fertilization

For *in vitro* fertilization, female B6D2F1 mice (Japan SLC) were superovulated by intraperitoneal injection of an anti-inhibin antiserum solution (CARD HyperOva, Kyudo); after 46-48 h, an intraperitoneal injection of 5 IU human chorionic gonadotropin (hCG, ASKA Animal Health) was performed. Cumulus-oocyte complexes were collected at 13-15 h after hCG injection, cultured in CARD mHTF medium (Kyudo), and inseminated with 1×10^5 cells/ml of capacitated sperm collected from the cauda epididymis of >12-week-old B6D2F1 male mice for 90 min. The eggs were washed three times and then cultured in the CARD KSOM medium. One-cell embryos were collected at 4 h after the beginning of the insemination step and used for microinjection. All the embryo culture was performed in paraffin oil (26117-45; Nacalai Tesque) in an atmosphere of 5% CO_2 in air at 37°C.

Identification of oocyte proteins by LC-MS/MS analysis

Approximately 200 zona-free oocytes from B6D2F1 mice were lysed in 6 M guanidine-HCl containing 100 mM HEPES-NaOH (pH 8.0), 10 mM Tris (2-carboxyethyl) phosphine and 40 mM chloroacetamide. The lysates were dissolved by heating and sonication and cleared by centrifugation at 20,000 ***g*** for 15 min at 4°C. Proteins were purified by methanol/chloroform precipitation and solubilized using 0.1% RapiGest SF (186002122; Waters) in 50 mM triethylammonium bicarbonate. The proteins were digested with 200 ng of trypsin/Lys-C mix (V5071; Promega) for 16 h at 37°C. The digests were acidified and desalted using GL-Tip SDB (7820-11200; GL Sciences). The eluates were evaporated in a SpeedVac concentrator and dissolved in 0.1% trifluoroacetic acid and 3% acetonitrile (ACN). Liquid chromatography (LC)-mass spectrometry (MS)/MS analysis of the resultant peptides was performed on an EASY-nLC 1200 UHPLC connected to a Q Exactive Plus mass spectrometer through a nanoelectrospray ion source (Thermo Fisher Scientific). The peptides were separated in a 75 µm inner diameter×150 mm C18 reversed-phase column (Nikkyo Technos) with a linear gradient from 4 to 32% ACN for 100 min followed by an increase to 80% ACN for 10 min. The mass spectrometer was operated in data-dependent acquisition mode with the top 10 MS/MS method. MS1 spectra were measured with a resolution of 70,000, an AGC target of 1×10^6 and a mass range of 350-1500 m/*z*. The MS/MS spectra were triggered at a resolution of 17,500, an AGC target of 5.0×10^4, an isolation window of 2.0 m/*z*, a maximum injection time of 60 ms and a normalized collision energy of 27 eV. Dynamic exclusion was set to 15 s. Raw data were directly analyzed against the SwissProt database restricted to *Mus musculus* using Proteome Discoverer version 2.3 (Thermo Fisher Scientific) with Mascot search engine version 2.5 (Matrix Science). The search parameters were as follows: (1) trypsin as an enzyme with up to two missed cleavages; (2) precursor mass tolerance of 10 ppm; (3) fragment mass tolerance of 0.02 Da; (4) carbamidomethylation of cysteine as a fixed modification; and (5) acetylation of protein N-terminus and oxidation of methionine as variable modifications. Peptides and proteins were filtered at a false discovery rate (FDR) of 1% using the percolator node and the protein FDR validator node, respectively. Prediction of transmembrane domain was performed using TMHMM method (Krogh et al., 2001).

Inhibitor assays

After insemination and microinjection, fertilized eggs were cultured in KSOM medium. The formation of punctate structures was assayed as follows: embryos at 8 hpf were cultured in KSOM medium containing 100 nM PMA or DMSO (control) at the same dilution rate (0.5% vol/vol) for 10 h. The embryos at 20 hpf were cultured in KSOM medium containing 100 nM Pitstop2, 2 µM Staurosporine, or DMSO (control) at the same dilution rate (0.5% vol/vol) for 18 h. Fluorescent confocal images were acquired using a CV1000 microscope. Developmental ability was assayed as follows: Pitstop2 or DMSO at the concentration described above was supplemented after the establishment of each stage (at 8 hpf for the pronuclear stage, at 24 hpf for the two-cell stage or at 48 hpf for the four-cell stage), and the drugs were freshly supplemented every 24 h. Developmental

rates were examined by calculating the percentage of embryos reaching each stage at a certain time (24, 48, 54, 72 or 96 hpf for the two-, four-, eight-cell, morula or blastocyst stages, respectively). Dynasore treatment at the two-cell stage was carried out by culturing two-cell embryos at 24 hpf with KSOM medium containing 200 µM Dynasore or DMSO at the same dilution rate (0.5% vol/vol) to 48 hpf.

Three-dimensional object count and colocalization analysis

Three-dimensional object count and object-based colocalization analysis for the punctate structures were performed using the JACoP and 3D Objects Counter plugin in the ImageJ Fiji software (Bolte and Cordelieres, 2006; Schindelin et al., 2012). Images acquired using a CV1000 confocal microscope were used for the analysis. First, to obtain a relatively uniform and stable fluorescence intensity, confocal image stacks of 21 *z*-axis planes from the bottom (adjacent to the objective lens) were selected for each embryo, and background subtraction with a rolling ball radius of 10 pixels, followed by the application of a Gaussian blur filter with a radius of 1 pixel, were performed using Fiji software. Then, thresholding of fluorescent intensities was carried out as macro, and manually and modestly adjusted to fit the expression level of each embryo. A limit size filter of 10-5000 pixels was applied to reconstruct 3D objects. The number of colocalized centers of mass-particle coincidences was presented as the number of colocalized particles.

Statistical analysis

Statistical analyses were performed using IBM SPSS Statistics (version 26.0, SPSS). Data were compared using the two-tailed unpaired Student's *t*-test. Statistical significance is represented as *P<0.05, unless otherwise stated.

References

Anas, M.-K., Hammer, M.-A., Lever, M., Stanton, J.-A. L. and Baltz, J. M. (2007). The organic osmolytes betaine and proline are transported by a shared system in early preimplantation mouse embryos. *J. Cell. Physiol.* **210**, 266-277. doi:10.1002/jcp.20872

Baltz, J. M. and Zhou, C. (2012). Cell volume regulation in mammalian oocytes and preimplantation embryos. *Mol. Reprod. Dev.* **79**, 821-831. doi:10.1002/mrd.22117

Barrera, S. P., Castrejon-Tellez, V., Trinidad, M., Robles-Escajeda, E., Vargas-Medrano, J., Varela-Ramirez, A. and Miranda, M. (2015). PKC-dependent GlyT1 ubiquitination occurs independent of phosphorylation: inespecificity in lysine selection for ubiquitination. *PLoS ONE* **10**, e0138897. doi:10.1371/journal.pone.0138897

Bolte, S. and Cordelieres, F. P. (2006). A guided tour into subcellular colocalization analysis in light microscopy. *J. Microsc.* **224**, 213-232. doi:10.1111/j.1365-2818.2006.01706.x

Collado-Fernandez, E., Picton, H. M. and Dumollard, R. (2012). Metabolism throughout follicle and oocyte development in mammals. *Int. J. Dev. Biol.* **56**, 799-808. doi:10.1387/ijdb.120140ec

Doherty, G. P., Bailey, K. and Lewis, P. J. (2010). Stage-specific fluorescence intensity of GFP and mCherry during sporulation In Bacillus Subtilis. *BMC Res. Notes* **3**, 303. doi:10.1186/1756-0500-3-303

Dumollard, R., Carroll, J., Duchen, M. R., Campbell, K. and Swann, K. (2009). Mitochondrial function and redox state in mammalian embryos. *Semin. Cell Dev. Biol.* **20**, 346-353. doi:10.1016/j.semcdb.2008.12.013

Fernández-Sánchez, E., Martínez-Villarreal, J., Giménez, C. and Zafra, F. (2009). Constitutive and regulated endocytosis of the glycine transporter GLYT1b is controlled by ubiquitination. *J. Biol. Chem.* **284**, 19482-19492. doi:10.1074/jbc.M109.005165

Fujimuro, M. and Yokosawa, H. (2005). Production of antipolyubiquitin monoclonal antibodies and their use for characterization and isolation of polyubiquitinated proteins. *Methods Enzymol.* **399**, 75-76. doi:10.1016/S0076-6879(05)99006-X

Guastella, J., Brecha, N., Weigmann, C., Lester, H. A. and Davidson, N. (1992). Cloning, expression, and localization of a rat brain high-affinity glycine transporter. *Proc. Natl. Acad. Sci. USA* **89**, 7189-7193. doi:10.1073/pnas.89.15.7189

Haass, N. K., Kartenbeck, M. A. and Leube, R. E. (1996). Pantophysin is a ubiquitously expressed synaptophysin homologue and defines constitutive transport vesicles. *J. Cell Biol.* **134**, 731-746. doi:10.1083/jcb.134.3.731

Hadi, T., Hammer, M.-A., Algire, C., Richards, T. and Baltz, J. M. (2005). Similar effects of osmolarity, glucose, and phosphate on cleavage past the 2-cell stage in mouse embryos from outbred and F1 hybrid females. *Biol. Reprod.* **72**, 179-187. doi:10.1095/biolreprod.104.033324

Hasegawa, H., Utsunomiya, Y., Kishimoto, K., Yanagisawa, K. and Fujita, S. (1996). SFA-1, a novel cellular gene induced by human T-cell leukemia virus type 1, is a member of the transmembrane 4 superfamily. *J. Virol.* **70**, 3258-3263. doi:10.1128/jvi.70.5.3258-3263.1996

Kandasamy, P., Gyimesi, G., Kanai, Y. and Hediger, M. A. (2018). Amino acid transporters revisited: New views in health and disease. *Trends Biochem. Sci.* **43**, 752-789. doi:10.1016/j.tibs.2018.05.003

Krogh, A., Larsson, B., von Heijne, G. and Sonnhammer, E. L. L. (2001). Predicting transmembrane protein topology with a hidden Markov model: application to complete genomes. *J. Mol. Biol.* **305**, 567-580. doi:10.1006/jmbi.2000.4315

Langemeyer, L., Fröhlich, F. and Ungermann, C. (2018). Rab GTPase function in endosome and lysosome biogenesis. *Trends Cell Biol.* **28**, 957-970. doi:10.1016/j.tcb.2018.06.007

Lineberry, N., Su, L., Soares, L. and Fathman, C. G. (2008). The single subunit transmembrane E3 ligase gene related to anergy in lymphocytes (GRAIL) captures and then ubiquitinates transmembrane proteins across the cell membrane. *J. Biol. Chem.* **283**, 28497-28505. doi:10.1074/jbc.M805092200

Liu, Q. R., López-Corcuera, B., Mandiyan, S., Nelson, H. and Nelson, N. (1993). Cloning and expression of a spinal cord- and brain-specific glycine transporter with novel structural features. *J. Biol. Chem.* **268**, 22802-22808. doi:10.1016/S0021-9258(18)41598-0

Mayor, S., Parton, R. G. and Donaldson, J. G. (2014). Clathrin-independent pathways of endocytosis. *Cold Spring Harb. Perspect. Biol.* **6**, a016758. doi:10.1101/cshperspect.a016758

Miyado, K., Yoshida, K., Yamagata, K., Sakakibara, K., Okabe, M., Wang, X., Miyamoto, K., Akutsu, H., Kondo, T., Takahashi, Y. et al. (2008). The fusing ability of sperm is bestowed by CD9-containing vesicles released from eggs in mice. *Proc. Natl. Acad. Sci. USA* **105**, 12921-12926. doi:10.1073/pnas.0710608105

Pelland, A. M. D., Corbett, H. E. and Baltz, J. M. (2009). Amino Acid transport mechanisms in mouse oocytes during growth and meiotic maturation. *Biol. Reprod.* **81**, 1041-1054. doi:10.1095/biolreprod.109.079046

Richard, S., Tartia, A. P., Boison, D. and Baltz, J. M. (2017). Mouse oocytes acquire mechanisms that permit independent cell volume regulation at the end of oogenesis. *J. Cell. Physiol.* **232**, 2436-2446. doi:10.1002/jcp.25581

Rink, J., Ghigo, E., Kalaidzidis, Y. and Zerial, M. (2005). Rab conversion as a mechanism of progression from early to late endosomes. *Cell* **122**, 735-749. doi:10.1016/j.cell.2005.06.043

Sakaguchi, A., Sato, M., Sato, K., Gengyo-Ando, K., Yorimitsu, T., Nakai, J., Hara, T., Sato, K. and Sato, K. (2015). REI-1 is a guanine nucleotide exchange factor regulating RAB-11 localization and function in C. elegans embryos. *Dev. Cell* **35**, 211-221. doi:10.1016/j.devcel.2015.09.013

Sato, K., Sato, M., Audhya, A., Oegema, K., Schweinsberg, P. and Grant, B. D. (2006). Dynamic regulation of caveolin-1 trafficking in the germ line and embryo of Caenorhabditis elegans. *Mol. Biol. Cell* **17**, 3085-3094. doi:10.1091/mbc.e06-03-0211

Sato, M., Grant, B. D., Harada, A. and Sato, K. (2008). Rab11 is required for synchronous secretion of chondroitin proteoglycans after fertilization in Caenorhabditis elegans. *J. Cell Sci.* **121**, 3177-3186. doi:10.1242/jcs.034678

Sato, M., Konuma, R., Sato, K., Tomura, K. and Sato, K. (2014). Fertilization-induced K63-linked ubiquitylation mediates clearance of maternal membrane proteins. *Development* **141**, 1324-1331. doi:10.1242/dev.103044

Satouh, Y., Nozawa, K., Yamagata, K., Fujimoto, T. and Ikawa, M. (2017). Viable offspring after imaging of Ca^{2+} oscillations and visualization of the cortical reaction in mouse eggs. *Biol. Reprod.* **96**, 563-575. doi:10.1093/biolre/iox002

Schindelin, J., Arganda-Carreras, I., Frise, E., Kaynig, V., Longair, M., Pietzsch, T., Preibisch, S., Rueden, C., Saalfeld, S., Schmid, B. et al. (2012). Fiji: an open-source platform for biological-image analysis. *Nat. Methods* **9**, 676-682. doi:10.1038/nmeth.2019

Shin, S.-W., Shimizu, N., Tokoro, M., Nishikawa, S., Hatanaka, Y., Anzai, M., Hamazaki, J., Kishigami, S., Saeki, K., Hosoi, Y. et al. (2013). Mouse zygote-specific proteasome assembly chaperone important for maternal-to-zygotic transition. *Biol Open* **2**, 170-182. doi:10.1242/bio.20123020

Steeves, C. L., Hammer, M.-A., Walker, G. B., Rae, D., Stewart, N. A. and Baltz, J. M. (2003). The glycine neurotransmitter transporter GLYT1 is an organic osmolyte transporter regulating cell volume in cleavage-stage embryos. *Proc. Natl. Acad. Sci. USA* **100**, 13982-13987. doi:10.1073/pnas.2334537100

Tartia, A. P., Rudraraju, N., Richards, T., Hammer, M.-A., Talbot, P. and Baltz, J. M. (2009). Cell volume regulation is initiated in mouse oocytes after ovulation. *Development* **136**, 2247-2254. doi:10.1242/dev.036756

Toralova, T., Kinterova, V., Chmelikova, E. and Kanka, J. (2020). The neglected part of early embryonic development: maternal protein degradation. *Cell. Mol. Life Sci.* **77**, 3177-3194. doi:10.1007/s00018-020-03482-2

Tsukamoto, S., Kuma, A., Murakami, M., Kishi, C., Yamamoto, A. and Mizushima, N. (2008). Autophagy is essential for preimplantation development of mouse embryos. *Science* **321**, 117-120. doi:10.1126/science.1154822

Tsukamoto, S., Hara, T., Yamamoto, A., Ohta, Y., Wada, A., Ishida, Y., Kito, S., Nishikawa, T., Minami, N., Sato, K. et al. (2013). Functional analysis of lysosomes during mouse preimplantation embryo development. *J. Reprod. Dev.* **59**, 33-39. doi:10.1262/jrd.2012-096

Umeda, R., Satouh, Y., Takemoto, M., Nakada-Nakura, Y., Liu, K., Yokoyama, T., Shirouzu, M., Iwata, S., Nomura, N., Sato, K. et al. (2020). Structural insights into tetraspanin CD9 function. *Nat. Commun.* **11**, 1606. doi:10.1038/s41467-020-15459-7

Van Wijk, S. J. L., Fulda, S., Dikic, I. and Heilemann, M. (2019). Visualizing ubiquitination in mammalian cells. *EMBO Rep.* **20**, e46520. doi:10.15252/embr.201846520

Van Winkle, L. J., Haghighat, N., Campione, A. L. and Gorman, J. M. (1988). Glycine transport in mouse eggs and preimplantation conceptuses. *Biochim. Biophys. Acta* **941**, 241-256. doi:10.1016/0005-2736(88)90185-X

Van Winkle, L. J., Campione, A. L., Gorman, J. M. and Weimer, B. D. (1990). Changes in the activities of amino acid transport systems $b^{0,+}$ and L during development of preimplantation mouse conceptuses. *Biochim. Biophys. Acta* **1021**, 77-84. doi:10.1016/0005-2736(90)90387-4

Van Winkle, L. J., Mann, D. F., Wasserlauf, H. G. and Patel, M. (1992). Mediated Na(+)-independent transport of L-glutamate and L-cystine in 1- and 2-cell mouse conceptuses. *Biochim. Biophys. Acta* **1107**, 299-304. doi:10.1016/0005-2736(92)90416-J

Van Winkle, L. J., Patel, M., Wasserlauf, H. G., Dickinson, H. R. and Campione, A. L. (1994). Osmotic regulation of taurine transport via system β and novel processes in mouse preimplantation conceptuses. *Biochim. Biophys. Acta* **1191**, 244-255. doi:10.1016/0005-2736(94)90175-9

Vargas-Medrano, J., Castrejon-Tellez, V., Plenge, F., Ramirez, I. and Miranda, M. (2011). PKCβ-dependent phosphorylation of the glycine transporter 1. *Neurochem. Int.* **59**, 1123-1132. doi:10.1016/j.neuint.2011.08.006

Verlhac, M.-H., Terret, M.-E. and Pintard, L. (2010). Control of the oocyte-to-embryo transition by the ubiquitin-proteolytic system in mouse and *C. elegans*. *Curr Opin Cell Biol* **22**, 758-763. doi:10.1016/j.ceb.2010.09.003

von Kleist, L., Stahlschmidt, W., Bulut, H., Gromova, K., Puchkov, D., Robertson, M. J., MacGregor, K. A., Tomilin, N., Pechstein, A., Chau, N. et al. (2011). Role of the clathrin terminal domain in regulating coated pit dynamics revealed by small molecule inhibition. *Cell* **146**, 471-484. doi:10.1016/j.cell.2011.06.025

Wang, Q.-C., Liu, J., Duan, X., Cui, X.-S., Kim, N.-H., Xiong, B. and Sun, S.-C. (2015). The Dynamin 2 inhibitor Dynasore affects the actin filament distribution during mouse early embryo development. *J. Reprod. Dev.* **61**, 49-53. doi:10.1262/jrd.2014-079

Yamagata, K., Suetsugu, R. and Wakayama, T. (2009). Long-term, six-dimensional live-cell imaging for the mouse preimplantation embryo that does not affect full-term development. *J. Reprod. Dev.* **55**, 343-350. doi:10.1262/jrd.20166
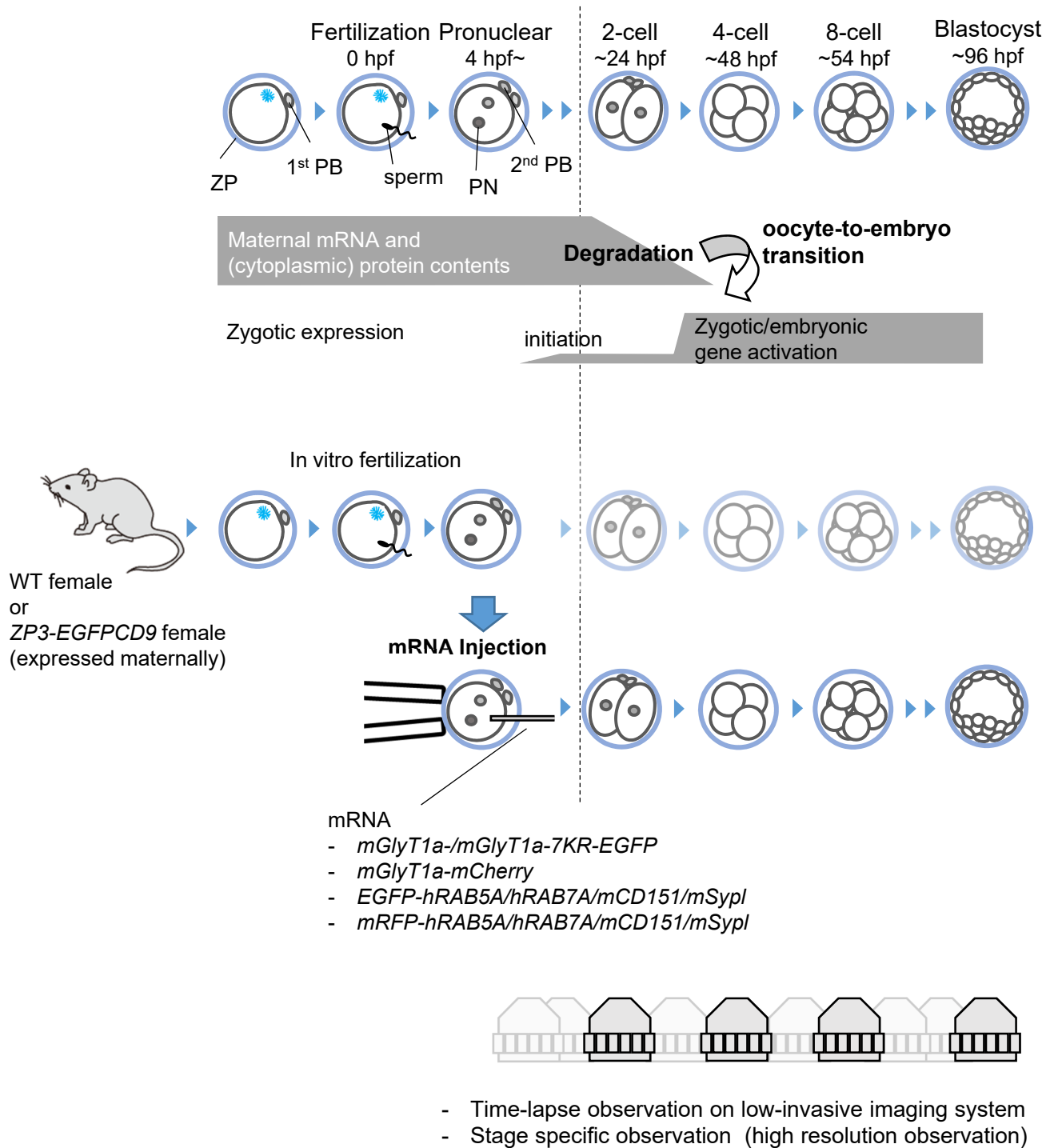
Fig. S1. Schematic summary of experimental system used in this study.
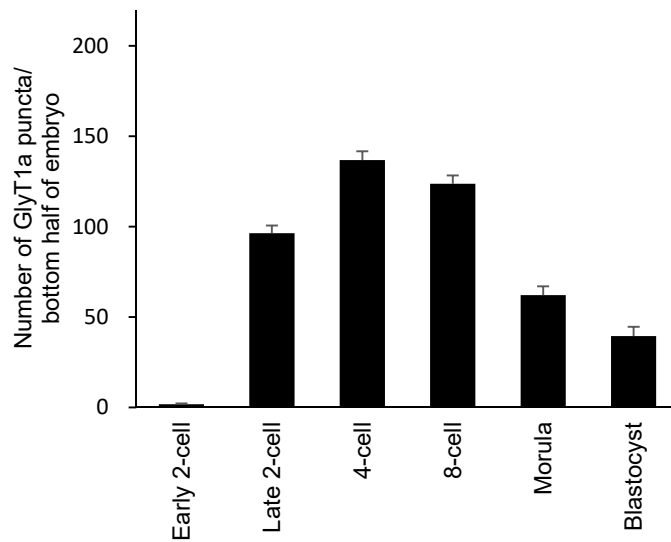ZP: Zona pellucida, PB: Polar body, PN: pronuclear.

Fig. S2. GlyT1a punctate structures emerge at the late 2-cell stage. Embryos microinjected with m*GlyT1a-mCherry* mRNA were cultured to the indicated stages. The number of GlyT1a-mCherry–positive puncta per half embryo. The error bars indicate s.e.m.
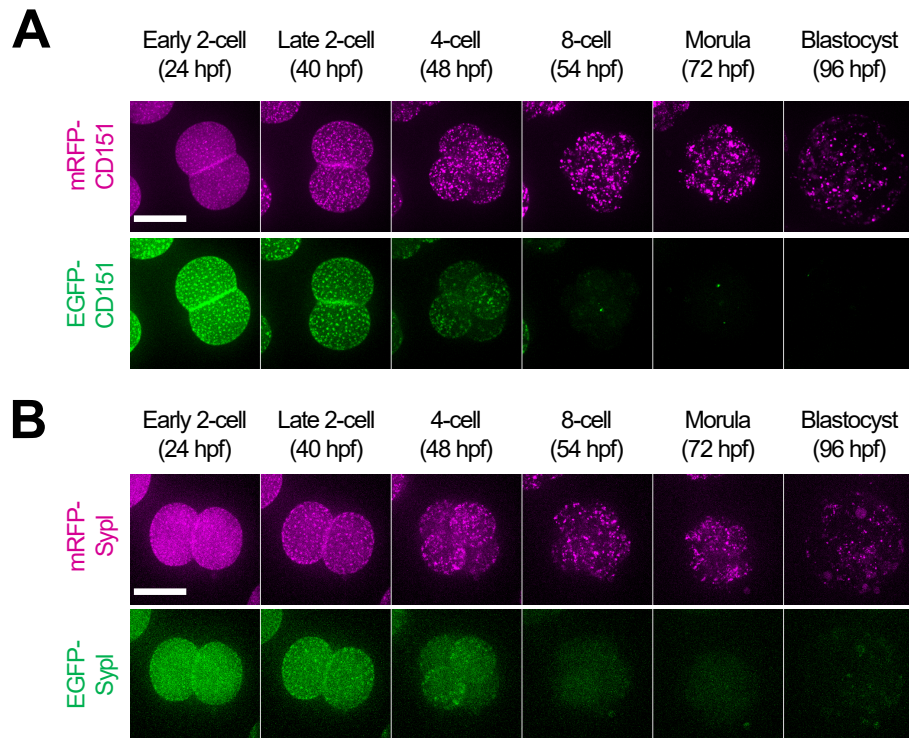
Fig. S3. Plasma membrane proteins are endocytosed in a time-specific manner during embryogenesis. Embryos expressing EGFP-CD151 and mRFP-CD151(A) or EGFP-Sypl and mRFP-Sypl(B) were continuously observed via a low-invasive imaging system. The maximum intensity projections of same embryo are indicated. Scale bar: 50 µm.
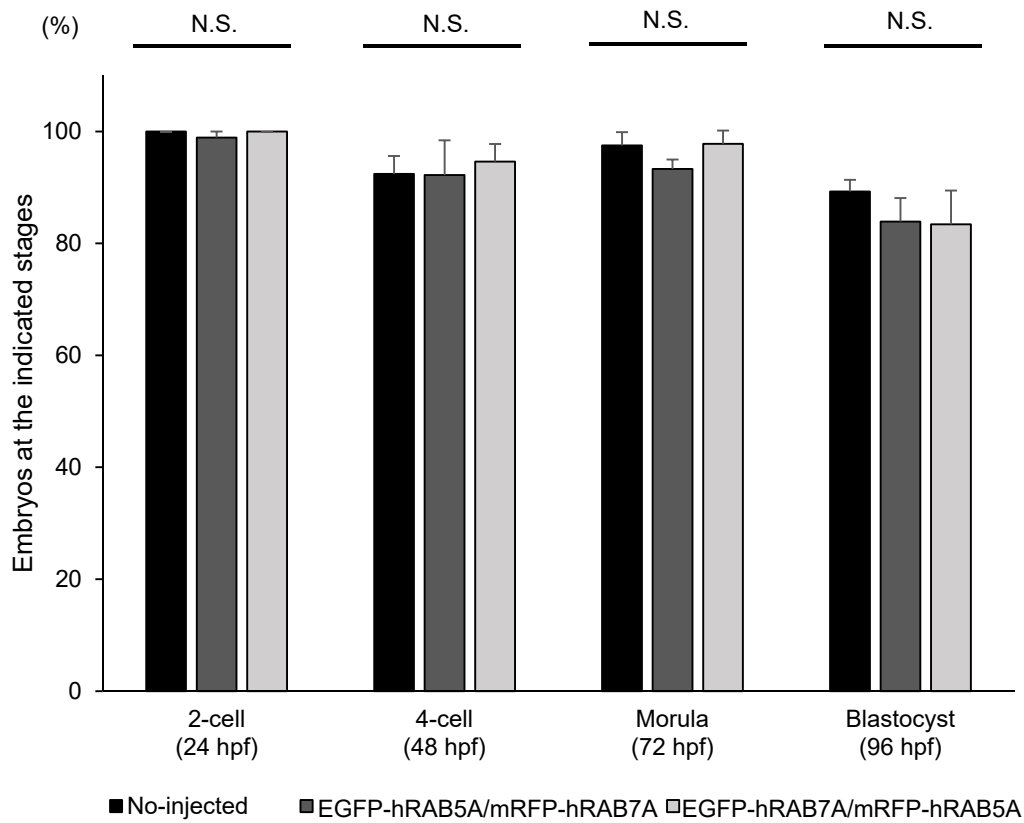
Fig. S4. Distributions of embryonic development at each time point. Embryos microinjected with mixed mRNA of *EGFP-hRAB5A* and *mRFP-hRAB7A*, mixed mRNA of *EGFP-hRAB7A* and *mRFP-hRAB5A*, or non-injected were cultured to the indicated time points. The error bars indicate s.e.m.
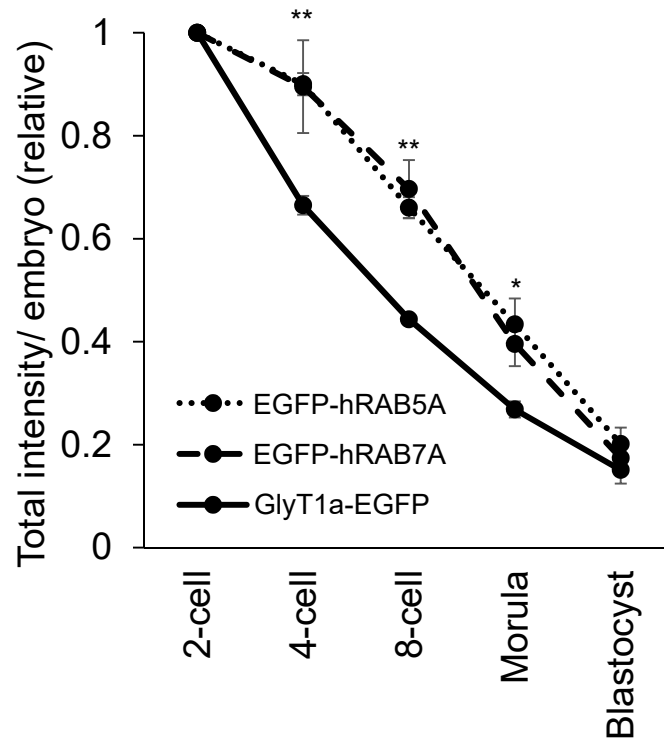
Fig. S5. Relative fluorescent levels of whole embryos at each stage. Relative fluorescent levels in the average intensity projection images of whole embryos expressing EGFP-hRAB5A, EGFP-hRAB7A, or mGlyT1a-EGFP at the indicated stages. Data are representative of three independent experiments. The error bars indicate s.e.m.
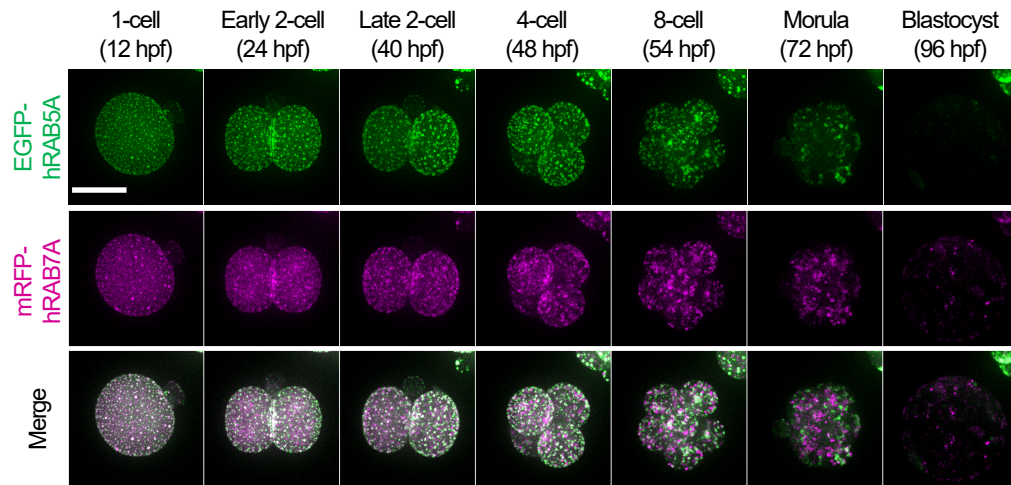
Fig. S6. Endosomal maturation is developmentally regulated during embryogenesis.
Embryos expressing EGFP-hRAB5A and mRFP-hRAB7A were continuously observed via a low-invasive imaging system. The maximum intensity projections of same embryo are indicated. Scale bar: 50 µm.
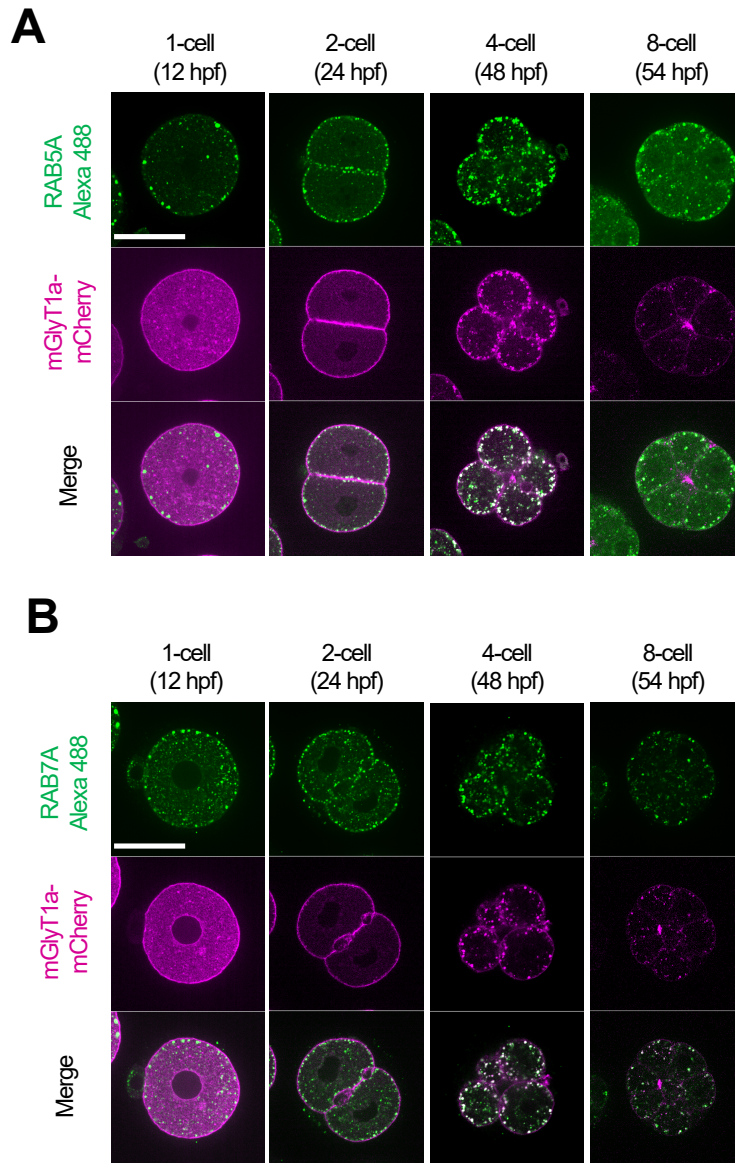
Fig. S7. GlyT1a is endocytosed via endogenous RAB5 and RAB7. (A) Embryos expressing mGlyT1a-mCherry were cultured to the indicated stages, stained with anti-RAB5 antibody(A) or -RAB7 antibody(B) and observed using laser confocal fluorescence microscopy. Scale bar: 50 μm.
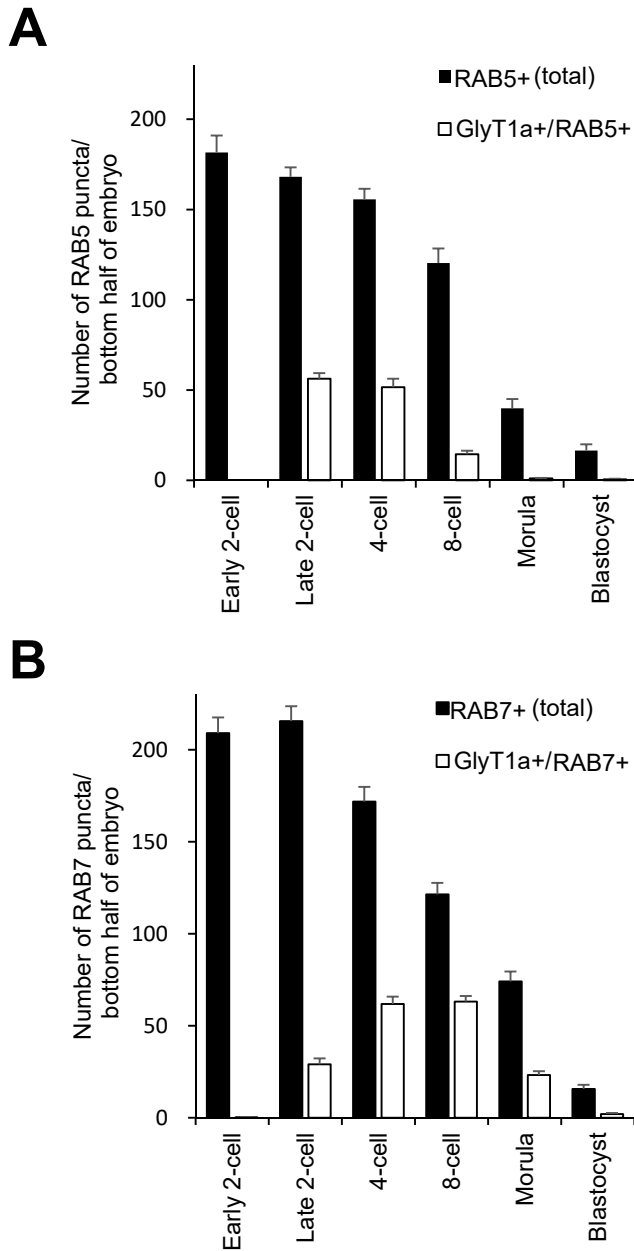
Fig. S8. GlyT1a colocalizes with endosome markers. Embryos microinjected with mRNAs were cultured to the indicated stages. (A, B) The numbers of EGFP-hRAB5A or -hRAB7A puncta per half embryo and the numbers of puncta colocalized with mGlyT1a-mCherry signals. The error bars indicate s.e.m.
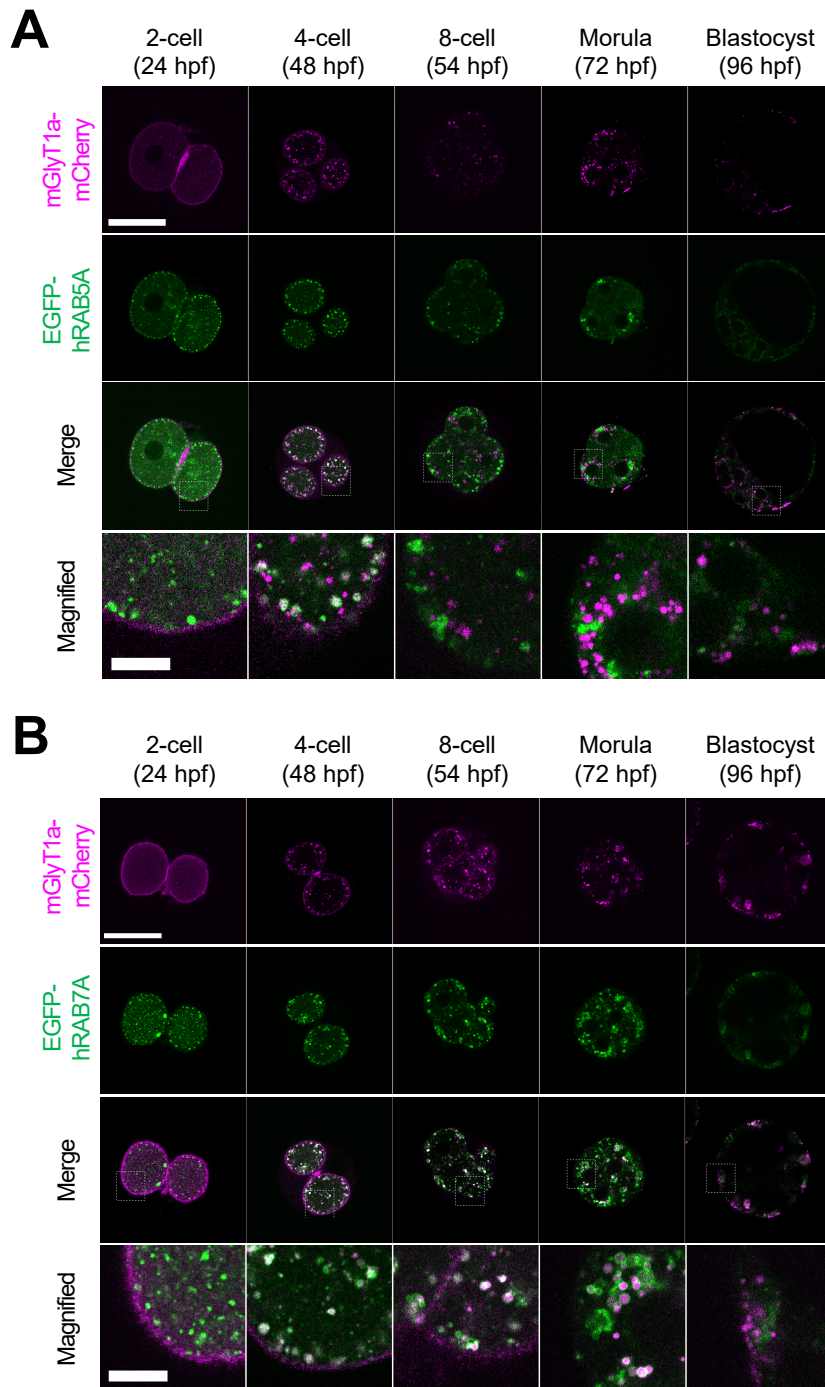
Fig. S9. GlyT1a localization changes from membranous to luminal during endocytosis. (A) Embryos expressing EGFP-hRAB5A and mGlyT1a-mCherry at the indicated stages. (B) Embryos expressing EGFP-hRAB7A and mGlyT1a-mCherry at the indicated stages. Embryos were observed by laser confocal fluorescence microscopy. Regions in the white dotted frame are magnified. Scale bar: 50 μm (magnified: 10 μm).
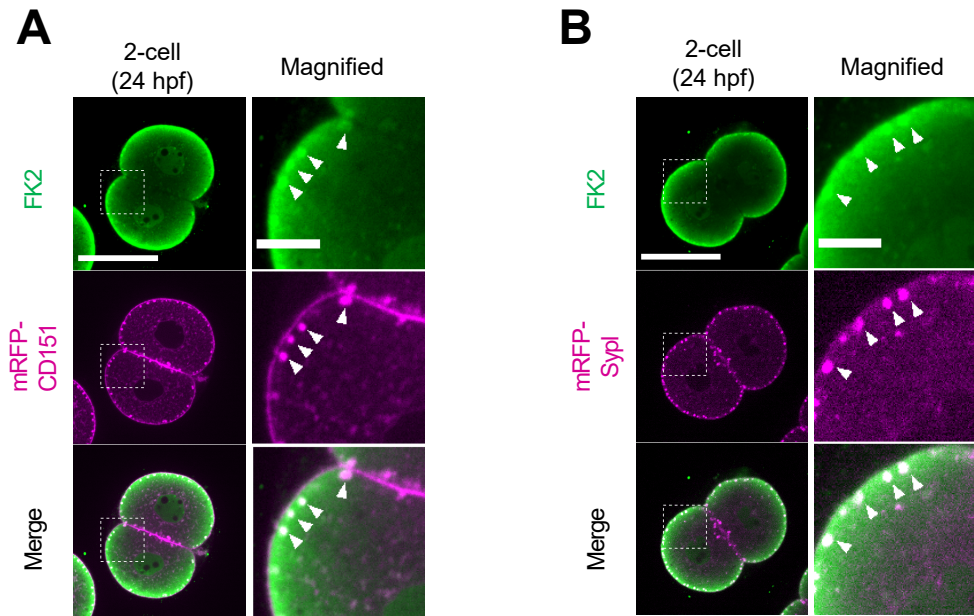
Fig. S10. Plasma membrane proteins are endocytosed via ubiquitination. Embryos expressing mRFP-CD151 (A) or mRFP-Sypl (B) were fixed and stained with an anti-ubiquitin antibody (FK2; green). The arrowheads indicate punctate structures showing accumulation and colocalization. Single confocal z-plane slices observed using laser confocal fluorescence microscopy are indicated. Scale bar: 50 µm (magnified: 10 µm).
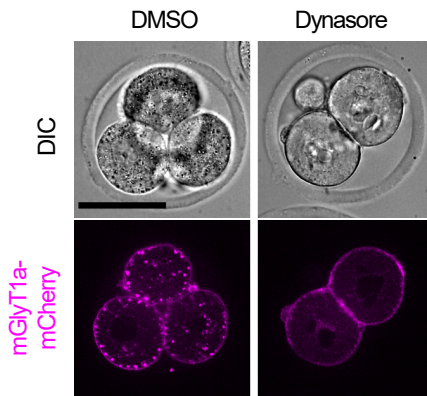
Fig. S11. Endocytosis of GlyT1a is inhibited by a dynamin inhibitor, Dynasore. Embryos expressing mGlyT1a-mCherry after treatment of Dynasore from 24 hpf to 48 hpf are observed. Single confocal z-plane slices are indicated. Scale bar: 50 μm.

Table S1. Identification of maternal transmembrane proteins on mouse oocyte. Zona-free 200 unfertilized oocytes from B6D2F1 females were solubilized for LC-MS/MS analysis. To select oocyte transmembrane proteins, the identified proteins with annotation of "membrane" on Proteome Discoverer program were selected, and transmembrane domain(s) were predicted using TMHMM (Krogh *et al.,* 2001). Proteins with one or more transmembrane domains are listed. *1: PSM=peptide spectrum match, *2: TMD=transmembrane domains, *3: analyzed in this study, *4: transgenic animal expressing N-terminally EGFP-tagged protein used in this study, *5: fluorescent protein-tagged proteins were tested by microinjection of mRNA, but weak expression.

	Gene Symbol	Gene Description	Proteomic analysis results		
			Number of PSMs *1	Number of Unique Peptides	Number of TMDs *2
1	*Ndufa4*	Cytochrome c oxidase subunit NDUFA4	6	5	1
2	*Sec22b*	Vesicle-trafficking protein SEC22b	5	5	1
3	*Pgrmc2*	Membrane-associated progesterone receptor component 2	5	5	1
4	*Htra2*	Serine protease HTRA2, mitochondrial	5	5	1
5	*Fam151a*	Protein FAM151A	7	6	1
6	*Usp30*	Ubiquitin carboxyl-terminal hydrolase 30	5	5	1
7	*Vamp3*	Vesicle-associated membrane protein 3	3	3	1
8	*Akap1*	A-kinase anchor protein 1, mitochondrial	3	3	1
9	*Ndufa13*	NADH dehydrogenase [ubiquinone] 1 alpha subcomplex subunit 13	3	2	1
10	*Pex11b*	Peroxisomal membrane protein 11B	3	3	1
11	*Cyb5*	Cytochrome b5	3	3	1
12	*Lman1*	Protein ERGIC-53	3	3	1
13	*Faah*	Fatty-acid amide hydrolase 1	3	3	1
14	*Sec61b*	Protein transport protein Sec61 subunit beta	3	2	1
15	*Cox6c*	Cytochrome c oxidase subunit 6C	3	3	1
16	*Ctsd*	Cathepsin D	3	3	1
17	*Aldh3a2*	Fatty aldehyde dehydrogenase	3	3	1
18	*Esyt1*	Extended synaptotagmin-1	2	2	1
19	*Letm1*	Mitochondrial proton/calcium exchanger protein	2	2	1
20	*Cyb5b*	Cytochrome b5 type B	2	2	1
21	*Pigt*	GPI transamidase component PIG-T	2	2	1
22	*Arhgap1*	Rho GTPase-activating protein 1	2	2	1
23	*Fkbp8*	Peptidyl-prolyl cis-trans isomerase FKBP8	2	2	1
24	*Hmox2*	Heme oxygenase 2	2	2	1
25	*Spast*	Spastin	2	2	1
26	*Slc3a2*	4F2 cell-surface antigen heavy chain	2	2	1
27	*Minos1*	MICOS complex subunit Mic10	2	2	1
28	*Lpcat1*	Lysophosphatidylcholine acyltransferase 1	2	2	1
29	*Timm50*	Mitochondrial import inner membrane translocase subunit TIM50	2	2	1
30	*Zfpl1*	Zinc finger protein-like 1	2	2	1
31	*Atp5j2*	ATP synthase subunit f, mitochondrial	2	2	1
32	*Mosc2*	Mitochondrial amidoxime reducing component 2	2	2	1
33	*Smco2*	Single-pass membrane and coiled-coil domain-containing protein 2	1	1	1
34	*Pex13*	Peroxisomal membrane protein PEX13	1	1	1
35	*Gxylt1*	Glucoside xylosyltransferase 1	1	1	1
36	*Itgae*	Integrin alpha-E	1	1	1
37	*Jag1*	Protein jagged-1	1	1	1
38	*Vcan*	Versican core protein	1	1	1
39	*Pgam5*	Serine/threonine-protein phosphatase PGAM5, mitochondrial	6	5	1
40	*Pex14*	Peroxisomal membrane protein PEX14	3	3	1
41	*Insrr*	Insulin receptor-related protein	2	1	1
42	*Emb*	Embigin	1	1	2
43	*Lrp8*	Low-density lipoprotein receptor-related protein 8	2	1	2
44	*Sema5b*	Semaphorin-5B	1	1	2
45	*Tmed2*	Transmembrane emp24 domain-containing protein 2	9	5	2

(continue to next page)

Table S1. (continued)

| Gene Symbol | Gene Description | Proteomic analysis results | | |
		Number of PSMs [*1]	Number of Unique Peptides	Number of TMDs [*2]
46 COX2	Cytochrome c oxidase subunit 2	8	5	2
47 Ninj1	Ninjurin-1	2	2	2
48 Bscl2	Seipin	4	3	2
49 Atp6ap2	Renin receptor	3	3	2
50 Reep5	Receptor expression-enhancing protein 5	2	2	2
51 Rabac1	Prenylated Rab acceptor protein 1	2	2	2
52 Sacm1l	Phosphatidylinositide phosphatase SAC1	2	2	2
53 Slc25a4	ADP/ATP translocase 1	15	5	3
54 Abcd3	ATP-binding cassette sub-family D member 3	2	2	3
55 Tmem14c	Transmembrane protein 14C	7	2	4
56 Arl6ip1	ADP-ribosylation factor-like protein 6-interacting protein 1	2	2	4
57 Cd151 [*3]	CD151 antigen	3	2	4
58 Cd9 [*4]	CD9 antigen	3	3	4
59 Sypl [*3]	Synaptophysin-like protein 1	6	2	4
60 Tspan14 [*5]	Tetraspanin-14	1	1	4
61 Sft2d2	Vesicle transport protein SFT2B	1	1	4
62 Zdhhc20	Palmitoyltransferase ZDHHC20	1	1	4
63 Surf4	Surfeit locus protein 4	3	2	5
64 Clptm1	Cleft lip and palate transmembrane protein 1 homolog	2	2	5
65 Aldh16a1	Aldehyde dehydrogenase family 16 member A1	1	1	5
66 Parl	Presenilins-associated rhomboid-like protein, mitochondrial	5	5	6
67 Cds1	Phosphatidate cytidylyltransferase 1	2	2	7
68 Grm8	Metabotropic glutamate receptor 8	1	1	7
69 Ano10	Anoctamin-10	2	2	8
70 Tm9sf2	Transmembrane 9 superfamily member 2	6	5	9
71 Slc11a2	Natural resistance-associated macrophage protein 2	2	2	9
72 Tm9sf3	Transmembrane 9 superfamily member 3	1	1	9
73 Stt3b	Dolichyl-diphosphooligosaccharide--protein glycosyltransferase subunit STT3B	3	3	10
74 Slc44a2	Choline transporter-like protein 2	1	1	10
75 Slc45a3	Solute carrier family 45 member 3	2	2	11
76 Slc12a9	Solute carrier family 12 member 9	3	3	11
77 Tmem168	Transmembrane protein 168	1	1	11
78 Npc1	NPC intracellular cholesterol transporter 1	2	2	12
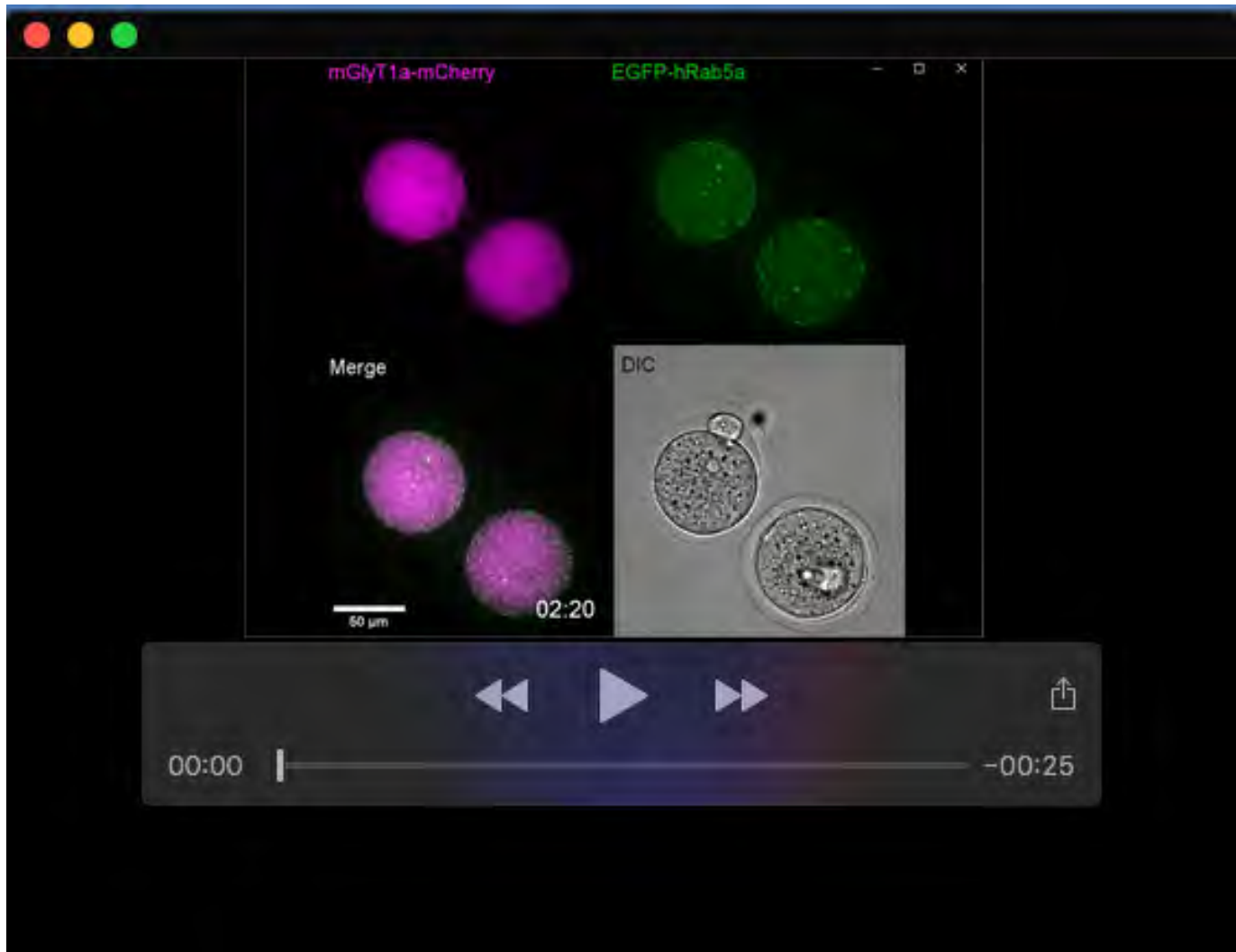
Movie 1. Time-lapse imaging of embryos expressing EGFP-hRAB5A and mGlyT1a-mCherry was performed to obtain DIC and fluorescent images at 8 hpf. Images were taken at intervals of 20 min to the blastocyst stage. The maximum intensity projections of the confocal micrographs are indicated. Scale bar: 50 μm.
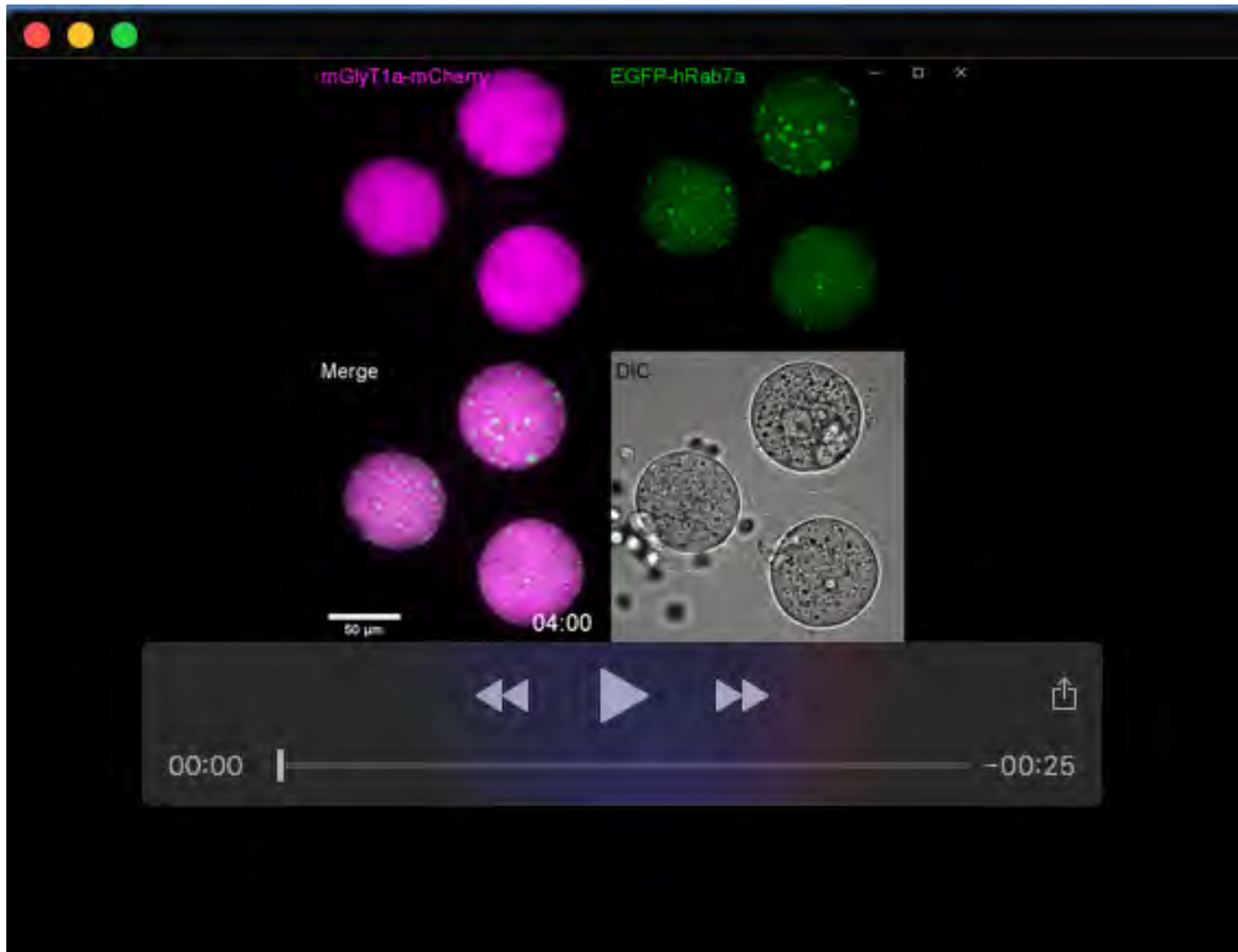
Movie 2. Time-lapse imaging of embryos expressing EGFP-hRAB7A and mGlyT1a-mCherry was performed to obtain DIC and fluorescent images at 8 hpf. Images were taken at intervals of 20 min to the blastocyst stage. The maximum intensity projections of the confocal micrographs are indicated. Scale bar: 50 μm.
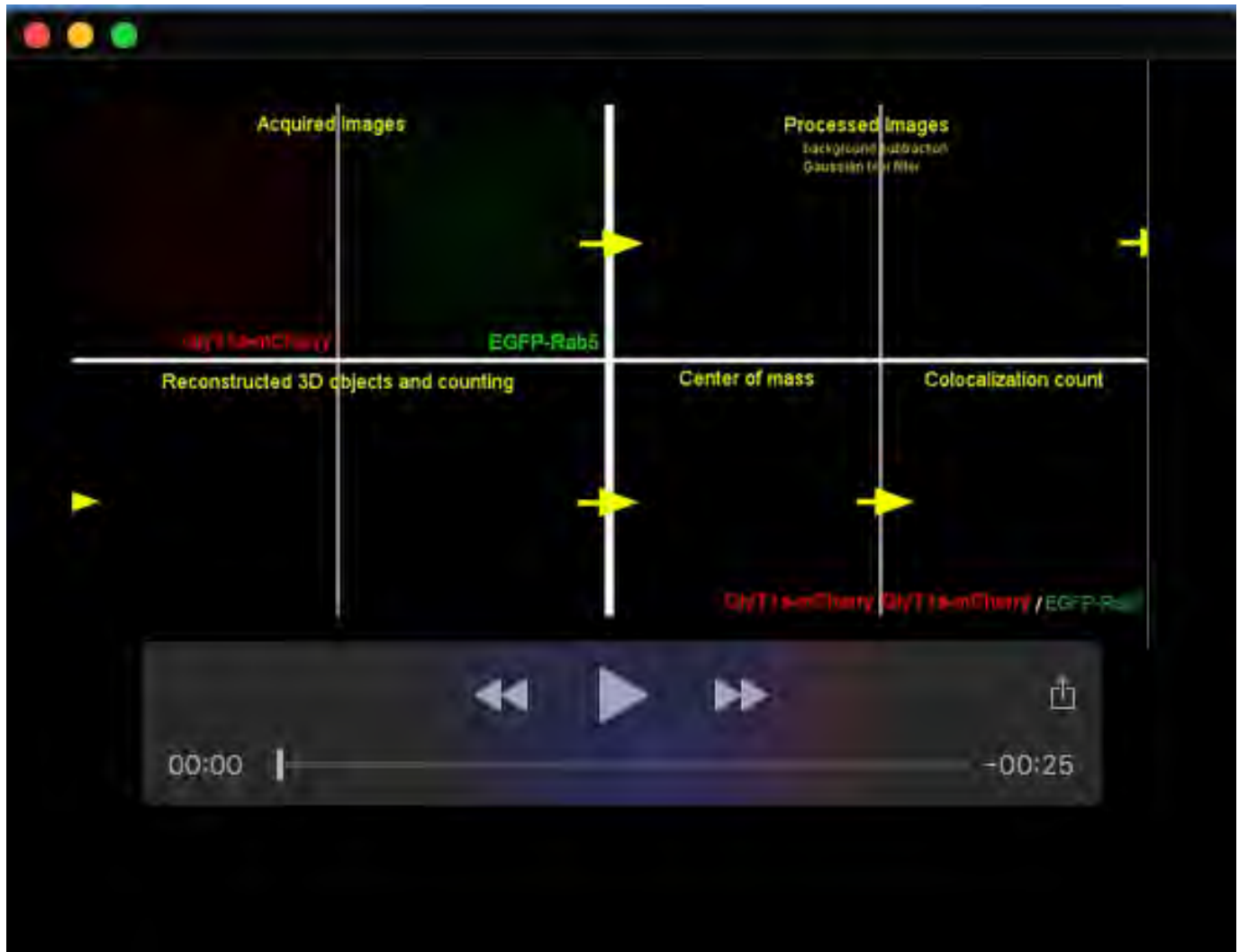
Movie 3. Counting of punctate structures and object-based co-localization analysis. Acquired confocal images of the bottom half of embryos (21 z-axis planes with 2 μm increments) for 488 nm (EGFP-hRAB5A) and 561 nm (mGlyT1a-mCherry) were processed with background subtraction and a Gaussian blur filter using Fiji software. Then, thresholding, three dimensional object reconstruction, and counting of the objects were processed on JACoP plugin of Fiji. The number of colocalized centers of mass (GlyT1a)-particle (RAB) coincidences was counted as the number of colocalized particles.